Onset and demise of coral reefs, relationship with regional ocean circulation on the Wyville Thomson Ridge

Mary Elliot, Christophe Colin, Mélanie Douarin, Edwige Pons-Branchu, Nadine Tisnerat-Laborde, Frédéric Schmidt, Elisabeth Michel, Quentin Dubois-Dauphin, Arnaud Dapoigny, Lorna Foliot, et al.

Onset and demise of coral reefs, relationship with regional ocean circulation on the Wyville Thomson Ridge

Authors : Mary Elliot[1*], Christophe Colin[2], Mélanie Douarin[1], Edwige Pons-Branchu[3], Nadine Tisnérat-Laborde[3], Frédéric Schmidt[2], Elisabeth Michel[3], Quentin Dubois-Dauphin[2], Arnaud Dapoigny[3], Lorna Foliot[3], Serge Miska[2], François Thil[3], Dave Long[4], Eric Douville[3]

1 Laboratoire de Planétologie/Géodynamique, UMR-CNRS 6112, Université de Nantes, Nantes, France.

2 Laboratoire GEOsciences Paris-Sud (GEOPS), Univ. Paris-Sud, CNRS, Université Paris-Saclay, Rue du Belvédère, Bât. 504, 91405 Orsay, France.

3 Laboratoire des Sciences du Climat et de l'Environnement, LSCE/IPSL, CEA-CNRS-UVSQ, Université Paris-Saclay, F-91191 Gif-sur-Yvette, France.

4 British Geological Survey, Currie EH14 4AP, Edinburgh, United Kingdom

* Corresponding author: mary.elliot@univ-nantes.fr

Abstract : Results from a vibrocore collected on the northern edge of the Scottish continental shelf at around 300 m water depth, on the Wyville Thomson Ridge, enable to reconstruct the history of cold water coral (CWC) reef growth and demise during the Holocene period. We report on significant age differences between U/Th and ^{14}C dates obtained on pristine well-preserved CWC (*Lophelia*

pertusa), which may reflect an diagenetic process that standard quality tests have failed to highlight. Additional ^{14}C dates derived from bivalve fragments (*Venus* sp.) and foraminifera (*Cibicides refulgens*) samples show a gradual ageing with core depth but with significant age inversions in the lower section of the sediment core, which we consider reflects sedimentary mixing. We thus chose to derive an independent age model using planktonic foraminifera *Globigerina bulloides* stable isotope profiles. The vibrocore record is divided into 3 phases: 1- Mixed sediment deposits of glacial age corresponding to the base of the core with ages older than 13 cal ka BP, 2- The end of the deglacial/early Holocene between 13-9 cal ka BP and 3- Finally, the Holocene period from around 9 cal ka BP with abundant *Lophelia pertusa* fossils. Siliciclastic grain size and clay mineralogical composition show two significant shifts at around 13 and 9 cal ka BP indicating changes in sedimentary sources and transport associated with the dynamics and flow patterns of surface currents during the deglaciation and Holocene. Our results show that the onset of CWC reef growth on the Wyville Thomson Ridge occurred around 9 cal ka BP and was associated with a shift in flow patterns of surface currents in this area. This change of circulation patterns induced favourable sedimentological and hydrological conditions for corals to grow, and is associated with large scale modifications of North Atlantic circulation patterns at the end of the deglaciation.

Introduction

A number of environmental factors such as temperature, salinity, density, oxygen availability, carbonate chemistry, food and nutrients and current velocity appear to control coral reef growth in tropical shallow-water zooxanthellate coral reefs (e.g. Veron, 1993; Dullo et al., 2008). However, the specific factors that control growth and settlement of non-zooxanthellate cold water coral (CWC) reefs have yet to be fully understood (Dorschel et al., 2007; White, 2007). These ecosystems were more recently discovered along the NW European continental margin (Dons, 1944; Le Danois, 1948; Teichert et al., 1958, Henriet et al., 1998). Over the past decades of exploration it has become clear that CWC have a world-wide distribution and *Lophelia pertusa* is one of the most common and widespread of the reef framework-forming cold-water corals (Roberts et al., 2006; 2009; Freiwald et al., 2004; 2017). These CWC ecosystems play a key role in marine biodiversity as they provide habitats for many other species. CWC ecosystems occur over a wide range of depth and within a specific range of temperature, salinity, density and physico-chemical conditions (Davies et al., 2008; Findlay et al., 2014; Robinson et al., 2014).

In the North-East Atlantic, CWC predominantly occur along the European continental margin, between ~100 and 1000 m water depth (Freiwald et al., 2004; 2017; Frank et al., 2011; Findlay et al., 2014; Dullo et al., 2008). Several environmental parameters are thought to be important for CWC reef growth in the

NE Atlantic. Seawater temperatures commonly range from 4 to 12°C, density is in the range of 27.35 to 27.65 kg m-3 (Dullo et al., 2008), and near bottom flow dynamics are energetic (Frederiksen et al., 1992; Freiwald, 2002; Kenyon et al., 2003; Roberts et al., 2009; Masson et al., 2003; Findlay et al., 2014). Finally, modern distributions of CWC seem to be strongly related to the supply of organic matter (Davies et al., 2009) and bottom currents that permit coral larvae dispersal, maintain (food) particles in suspension and prevent corals from being smothered by sediment (Mienis et al., 2007, 2009; Somoza et al., 2014; Sanchez et al., 2014).

Due to their critical role in modern marine ecosystems and the potential to use these archives for paleoenvironmental studies (e.g. Robinson et al., 2014) a number of key papers have attempted to understand and reconstruct the growth history of CWC reefs and mounds. These studies mainly based on U-series dating of fossil coral fragments retrieved from carbonate mounds have permitted to establish the late-Quaternary spatial and temporal distribution of CWC in the North Atlantic (Lutringer, 2003; Dorschel et al., 2005; Frank et al., 2009; 2011; López Correa et al., 2012; Douarin et al., 2013; Victorero et al., 2016; Bonneau et al., 2018). A number of growth models of carbonate mounds and reefs have been proposed (Wilson et al., 1979; Kenyon et al., 2003; De Mol et al.,2005; Dorschel et al., 2005; Roberts et al., 2006; Rüggeberg et al., 2007; De Haas et al., 2009; Bonneau et al., 2018; Pirlet et al., 2011). In more detail, it has been demonstrated that interglacial climates were favourable for CWC growth and

carbonate mound development, while until present no CWC from glacial periods have been discovered between 50°N and 70°N in the North Atlantic (Schröder-Ritzau et al., 2005; Van der Land et al., 2014; Frank et al., 2009; 2011; Douarin et al., 2013; Bonneau et al., 2018; Matos et al., 2015) nor at 25°N in the Gulf of Mexico (Matos et al., 2018). On the contrary, at temperate latitudes between 20°N and 50°N in the NE Atlantic, glacial periods are associated with increased framework forming CWC reef growth. *Lophelia pertusa* reef growth is reported during glacial periods and cool events such as the Younger Dryas in the Gulf of Cádiz, Mediterranean Sea and off Mauritania (Wienberg et al., 2009; 2010; McCulloch et al., 2010; Eisele et al., 2011; Frank et al., 2011).

Frank et al. (2011) has proposed that such glacial-interglacial changes in the distribution of CWC reefs in the North Atlantic could be linked to the North-South displacement of cold nutrient-rich intermediate waters and surface productivity driven by changes in the position of the polar front. However, other mechanisms could be involved in the emergence of this pattern, such as changes in the temperature and related pycnocline, which is associated with the development of nepheloid layers (Raddatz et al., 2014; Rüggeberg et al., 2016) or changes in detrital input (e.g. ice-rafted debris) (Pirlet et al., 2011; Thierens et al., 2012; Bonneau et al., 2018). The effect of the carbonate chemistry changes and pH and calcium carbonate saturation conditions of the ocean has been shown to have an effect on CWC growth (Hennige et al., 2015; Raddatz et al., 2016). More recently,

111 a compilation of U-series dating of CWC fragments collected in a restricted area
112 of the SW Rockall Trough margin have shown that CWC growth was influenced
113 by millennial-scale North Atlantic climate variability during the late Holocene
114 with systematic lower CWC occurrence during cold events of the late Holocene
115 (Bonneau et al., 2018). A similar study in Mingulay CWC reef also showed that
116 corals were sensitive to periods of rapid climate change (Douarin et al., 2015;
117 Dubois-Dauphin et al., 2019).
118
119 In this paper, we investigate a sedimentary record that provides new evidence for
120 the environmental parameters that control the settlement of CWC reefs on the
121 northern margin of the British continental shelf at the end of the last deglaciation.
122 A vibrocore was collected on the continental margin North of Scotland at 282 m
123 water depth. We obtained numerous U/Th and ^{14}C dates on *Lophelia pertusa* (12
124 of which are paired), and ^{14}C dates on bivalves (*Venus casima* and other *Venus*
125 sp.) and foraminifera (*Cibicides refulgens*). We also derived a stable isotope
126 profile from planktonic species *Globigerina bulloides*. Clay mineralogical
127 composition and laser grain-size distribution were measured in order to relate
128 changes in sediment sources and dynamic of transport with the appearance of the
129 CWC reef at this location.
130
131 2. Material and Methods
132

133 2.1 Sediment core location

134

135 The British Geological Survey (BGS) vibrocore +59-07/293VE was retrieved
136 from the UK continental shelf, at the junction with the Wyville Thomson Ridge
137 and the West Shetland shelf / Hebridean shelf (59°43.40N; 06°28.90W, 282 m
138 water depth) during a regional mapping survey on board the MV British
139 Enterprise Four (Long et al., 1999; (Figure 1)). Initial observations of CWC
140 presence at the study site were obtained in the 19th century (e.g. Wyville-
141 Thomson, 1874). More recently the area was surveyed and the distribution of
142 CWC mapped (Long et al., 1999). Results from this survey showed the presence
143 of living reefs of *Lophelia pertusa* down to a maximum water depth of 500 m with
144 a maximum presence of living reefs centred between 300-400 m (Roberts et al.,
145 2003; Long et al., 1999), but only dead CWC were observed at the study site.
146 Processes governing sedimentation in this area have been studied and show
147 complex interactions between bathymetry and bottom-water currents (Howe et
148 al., 2002).

149

150 The total recovery of vibrocore +59-07/293VE was 495 cm. Prior to sub-
151 sampling, the core was cut frozen with a diamond saw, in order to keep the internal
152 sedimentary structure intact. The top 300 cm of the core presented extremely
153 abundant fragments of *L. pertusa*, up to 9 cm length. A one meter section of the
154 core, between 61.5 to 161 cm, is highly disturbed with only small < 1 cm, highly

155 fragmented and eroded *L. pertusa* samples. The bottom section, from 300-495 cm,
156 presents no coral fragments. The biogenic fraction is composed of diverse
157 bivalves, benthic and planktonic foraminifera and numerous well-rounded
158 glaciomarine rock fragments. The coral-rich section of the core was sampled at
159 10 cm intervals, documenting the position and state of preservation of each coral
160 fragment. The bottom 195 cm of the core were sampled at 5 cm intervals. Clay
161 mineralogical analyses were performed on clay-sized fraction and laser grain-size
162 analyses were conducted after removal of carbonate and organic matter. Stable
163 isotopes ($\delta^{18}O$) of *Globigerina bulloides* were measured on sieved sediment
164 samples. U/Th and ^{14}C analyses were done on selected fragments of corals
165 sampled at specific depths down core.
166
167 2.2. Hydrological setting
168
169 The site investigated is located on the path of the North Atlantic Current (NAC)
170 (Figure 1). As the NAC flows northwards it mixes with the European Shelf Edge
171 Current (SEC) (Marsh et al., 2017; Inall et al., 2009; McCartney and Mauritzen,
172 2001). The SEC forms a northward-flowing boundary current centered at 200 m
173 depth that brings warm and saline upper water with Eastern North Atlantic Central
174 Water (ENACW) characteristics along the European margin to the Faroe-
175 Shetland Channel (Holliday et al., 2000; White and Bowyer, 1997; Hill and
176 Mitchelson-Jacob, 1992; Ellett et al., 1986; Pollard et al., 2004) (Figure 1). In

177 addition, the Scottish Coastal Current (SCC), which flows on the shelf margin,
178 mixes with SEC potentially indirectly affecting flow patterns at our study site
179 (Inall et al., 2009; Ellet et al. 1986, 1979). The Scottish Coastal Current (SCC)
180 brings cooler and fresher waters from the Irish and Clyde Seas (Ellett and
181 Edwards, 1983). In the deeper section of this channel colder waters flow: Arctic
182 Intermediate Waters (AIW) and Norwegian Sea Arctic Intermediate Waters
183 (NSAIW), which appear to control the lowest depth habitat of *L. pertusa* in this
184 area (Roberts et al., 2003).
185
186 2.3 Sampling for U/Th and ^{14}C dates
187
188 In total, 43 downcore pristine fossils of *L. pertusa* were selected for U/Th dating
189 (Table 1). A 3-4 g piece of each coral fragment was ultrasonically cleaned in
190 MilliQ water 3 times, as done in (Douarin et al., 2013), to avoid contamination
191 from sediment and surface deposit. Inner and outer surfaces of CWC samples
192 were carefully cleaned using a small diamond blade to avoid contamination from
193 iron and manganese oxides/hydroxides and surface sample re-crystallisation of
194 aragonite into calcite. The coral fragments were then sub-sampled for X-ray
195 diffraction (XRD) analysis for mineralogical analysis (aragonite content). The
196 XRD analysis was performed at GEOPS and confirmed that the cleaned corals
197 were made of 100% aragonite. Pristine coral samples were dated by ^{14}C and U-

198 series methods. The amount of material for each coral was larger than required to
199 account for potential duplicates or other analytic work.
200
201 2.4. AMS ^{14}C dates
202
203 Coral fragments are only present from the core top to 300 cm and thereafter
204 bivalves and foraminifera were used for ^{14}C dates. A total of 26 radiocarbon
205 Accelerator Mass Spectrometry (AMS) ages were obtained on a range of
206 material : 17 CWC, 3 marine bivalve fragments, 6 foraminifera *C. refulgens*
207 samples (Table 1). For each ^{14}C date about 10 mg of $CaCO_3$ is required. When
208 possible we used the subsamples of the same *L. pertusa* coral fragments used for
209 U/Th dates. For the foraminifera, specimens of benthic foraminifera *C. refulgens*
210 were hand-picked from the 250-1000 μm fraction of the sediment. Fragments of
211 marine bivalves (*Venus casima* and other *Venus* sp.) were selected and cleaned.
212 All ^{14}C ages were calibrated with CALIB 7 program using the calibration curve
213 Marine13 and assuming a mean constant surface ocean reservoir age of 400 years
214 (Stuiver et al., 2005; Reimer et al., 2013).
215
216 2.5. U/Th dates
217
218 The CWC fragments selected were U-series dated at the Laboratoire des Sciences
219 du Climat et de l'Environnement (LSCE, CEA-CNRS-UVSQ, Gif-sur-Yvette). 43

L. pertusa samples were analysed for uranium and thorium isotopes using a Multi-Collector Inductively Coupled Plasma Mass Spectrometer MC-ICP-MS. Prior to analyses, all fragments were examined under a binocular microscope to ensure against the presence of bio-eroded zones and finally crushed into a coarse-grained powder with an agate mortar and pestle. The powders (~60-200 mg) were transferred to acid cleaned Teflon beakers, ultrasonicated in MilliQ water, leached with 0.01 N HCl for around 15 s and finally rinsed twice with MilliQ water. The U and Th separation and purification followed a procedure modified from Pons-Branchu et al. (2005) and Douville et al. (2010). The physically and chemically cleaned samples were dissolved in 3-4 ml dilute HCl (~10%) and mixed with an internal triple spike with known concentrations of ^{229}Th, ^{233}U and ^{236}U, calibrated against a Harwell Uraninite solution (HU-1) assumed to be at secular equilibrium (Frank et al., 2004). After Fe-coprecipitation, the U and Th fractions were separated and purified on 600 µl columns packed with U-TEVA and prefilter resins in nitric media. The U and Th isotope ratios were determined using a Thermo ScientificTM MC-ICP-MS fitted with a desolvating introduction system (aridus II) following the procedure described by Pons-Branchu et al. (2014). The 230Th/U ages were calculated from measured atomic ratios through iterative age estimation (Ludwig and Titterington, 1994), using the ^{230}Th, ^{234}U and ^{238}U decay constants of Cheng et al. (2013) and Jaffey et al. (1971).

2.6. Stable isotopes: *G. bulloides* δ^{18}O and δ^{13}C profiles

About 10-20 specimens of *G. bulloides* (250-400 μm) were hand-picked at a 10 cm resolution from 0-300 cm and thereafter a 5 cm resolution. Samples were analysed at LSCE (CEA-CNRS-UVSQ, Gif-sur-Yvette) using an OPTIMA GV mass spectrometer with a common acid bath automatic preparation line. Shell oxygen isotope values are expressed relative to the isotopic ratio of the carbon dioxide gas derived from the Vienna Pee Dee Belemnite (VPDB) standard in conventional delta notation (δ). Ratios are reported in ‰ VPDB defined with respect to the NBS 19 ($\delta^{18}O$ = -2.20‰ VPDB), limestone standard. The mean external reproducibility (1) of carbonate standard is ±0.06% for $\delta^{18}O$ and ±0.04% for $\delta^{13}C$.

2.7. Clay mineralogical analyses

A total of 69 sediment samples collected from the vibrocore +59-07/293VE were used for clay mineralogical analyses. The clay minerals were identified by XRD using a PANalytical diffractometer at the GEOPS laboratory (Université Paris-Saclay, France) on oriented mounts of non-calcareous clay-sized (< 2 μm) particles. Briefly, deflocculation was accomplished by successive washing with distilled water after removing carbonate and organic matter by treating with acetic acid (25%) and hydrogen peroxide (15%), respectively. The particles smaller than

263 2 m were separated by sedimentation and centrifugation. Three XRD runs were
264 performed, following air-drying, ethylene-glycol solvation for 24 hours, and
265 heating at 490°C for 2 hours. The clay minerals were identified according to the
266 position of the (001) series of basal reflections on the three XRD diagrams. Mixed
267 layers composed mainly of smectite-illite (15-17 √Ö) were included in the
268 "smectite" category. Semi-quantitative estimates of peak areas of the basal
269 reflections for the main clay mineral groups of smectite (15-17 √Ö), illite (10 √Ö),
270 and kaolinite/chlorite (7 √Ö) were performed on the glycolated curve using the
271 MacDiff software. The relative proportions of kaolinite and chlorite were
272 determined based on the ratio from the 3.57/3.54 √Ö peak areas. The replicate
273 analyses of a few selected samples gave a precision of ¬±2% (2). Based on the
274 XRD method, the semi-quantitative evaluation of each clay mineral had an
275 accuracy of ~4%.
276
277 2.8. Laser grain-size analyses
278
279 Grain-size distribution measurements in the range of 0.02 to 2000 Œºm were
280 carried out on a Malvern Mastersizer 2000 Particle Size Analyzer on the same
281 samples as those analysed by XRD. Prior to the analyses, bulk sediment was pre-
282 treated with acetic acid (25%) and hydrogen peroxide (15%) to remove carbonates
283 and organic matter. The mixture was then rinsed several times with deionized

284 water and gently shaken to achieve disaggregation. The suspension was then
285 poured into the fluid module of the particle size analyser.
286
287 The total set of grain-size distributions (n=69) has been summarized by an
288 unmixing algorithm in order to estimate sediment sub-populations representing
289 different sources or dispersal processes. This approach has been significantly
290 improved by the last generation of unsupervised linear unmixing under positivity
291 and sum-to-one constraints (Weltje, 1997). We used the Bayesian Positive Source
292 Separation (BPSS) algorithm that has the main advantage of having robust
293 convergence properties (Moussaoui et al., 2006; Dobigeon et al., 2009; Schmidt
294 et al., 2010). We estimate both the grain-size distributions of each sub-population
295 (end-members) and the proportion of each end-member through time. The number
296 of end-members is estimated by the best trade-off between variance
297 reconstruction and end-member significance.
298
299 3. Results
300
301 3.1. Chronology and age model
302
303 All U/Th and ^{14}C dates are plotted against sediment core depth (Figure 2, (see also
304 Figure 4), Table 1, Table 2). A total of 43 U/Th and 17 ^{14}C dates were obtained
305 on *L. pertusa* samples from this sediment core. Additional ^{14}C dates were obtained

306 from 6 benthic foraminifera samples (*Cibicides refulgens*) and on 3 bivalves.
307 Results show that *L. pertusa* U/Th dates are spread more or less evenly downcore
308 and regularly increase from 2 to 8 ka BP down to 272 cm (Table 2). However,
309 after 272 cm U/Th dates start decreasing again to 5.6 ka at 306 cm (Table 2, Figure
310 2). Similarly, *L. pertusa* ^{14}C dates regularly increase from the core top to 310 cm
311 ranging from 2.5 to 8.45 cal ka BP. The *C. refulgens* ^{14}C dates also regularly
312 increase from 40 to 306 cm ranging from 5.4 to 10.3 cal ka BP. In the bottom
313 section of the core, from 385-480 cm, ^{14}C dates are much older 23-40.7 cal ka BP
314 (Table 1, Table 2, Figure 2). Finally, three ^{14}C dates were obtained from selected
315 samples of marine bivalves, *Venus casima* and *Venus* sp. The ages also increase
316 with depth from 10.7 at 308 cm to 27.4 at 425 cm. The sample selected at 480 cm
317 has an age older than 50 cal ka BP. We firstly observed an absence of well-
318 preserved coral fragments in the core from 61.5 to 160.5 cm and we were unable
319 to obtained reliable U/Th or ^{14}C dates. Secondly, we observed very significant age
320 offsets between the U/Th and the ^{14}C dates (Figure 2, Table 1, Table 2, Figure 4).
321
322 We conducted multiple analyses to test for any geochemical or physical alteration.
323 All the samples presented in this work have passed the standard checks for U/Th
324 and ^{14}C quality. Each sample was analysed for XRD and underwent thorough
325 cleaning and leaching procedures. Replicate analysis were conducted on several
326 samples for U/Th (Table 2), and we analysed twice the same solution (tests for
327 analytical reproducibility) and obtained similar ages. For the replicates at 293 cm

328 and 306 cm (Table 2), the U/Th analyses were done on different pieces of the
329 same coral. A little age difference around 140 years for the sample at 293 cm, or
330 more important around 400 years for sample 306 cm (5.20 ¬± 0.04 and 5.59 ¬±
331 0.03 ka BP, Table 2) is found for U/Th dating (Table 1). Similarly, the ^{14}C
332 analyses were run in two separate batches (starred and non-starred samples on
333 Table 1). Comparable results are found at similar depth: for example 4.8 cal ka
334 BP at 38.5cm and 4.7 cal ka BP at 39 cm; 8.4 cal ka BP at 268 cm and 8.4 cal ka
335 BP at 272 cm. Similar ages are also obtained for coral, foraminifera and bivalve
336 samples from the same sediment depth (for example *C. refulgens* at 250 cm at 8.2
337 cal ka BP and *L. pertusa* at 247cm at 8.4 cal ka BP). Based on all available data
338 and results, we conclude that there is no clear evidence for any geochemical or
339 physical alteration which may have explained the observed offset between U/Th
340 ages and ^{14}C ages.
341
342 Given that there appears to be an unexplainable significant discrepancy between
343 the U/Th ages and the ^{14}C ages, we decided to use the $\delta^{18}O$ profile as a guide to
344 build an age model. $\delta^{18}O$ values range from 2.5 to 1‰ from the base of the core
345 to the top (see Figure 4). These data are compared to a well-dated sediment core
346 from the North Atlantic (Na87-22, see Figure 5).
347
348 3.2. Siliciclastic grain size
349

350 Grain size of siliciclastic particles in vibrocore +59-07/293VE ranges from 0.6 to
351 800 ¬µm and the mean grain size varies from 19 to 100 ¬µm (average ~42 ¬µm)
352 (Figure 3). In general, the mean grain size presents higher values in the core
353 section 300-485 cm (Figure 3). The inversion algorithm for end-member
354 modelling of composition data for core +59-07/293VE displays a three end-
355 member model that explains more than 80% of the variance. The coarse end
356 member EM3 varies within the size range 0.6 to 800 ¬µm (bi-modal grain size of
357 ~5 and 110 ¬µm) (Figure 3). The intermediate end member EM1 varies in the size
358 range 2-141 ¬µm, with a modal grain size of ~20 ¬µm. The fine end-member
359 EM2 varies in the size range 1-141 ¬µm, and its modal grain size is ~6 ¬µm.
360 These last two end-members (EM1 and EM2) present a clearly defined unimodal
361 distribution. Relative contributions of the three end-members are plotted against
362 age in Figure 3. Proportions of the coarser end-member (EM3) display a large
363 range of variation, between 0 and 87%, with an average value of ~31%.
364 Proportions of the intermediate end-member (EM1) vary in a range, from 0 to
365 65% (average ~27%). The last end-member (EM2), which represents the finer
366 particles, varies between 0 and 80% (average 41%). The intermediate EM1
367 presents a higher percentage variability with no systematic change downcore.
368
369 The mean grain size is strongly influenced by the proportions of the coarse EM3
370 (Figure 3). The evolution of the proportion of EM1 and EM3 shows a significant
371 shift at around 300 cm. The coarser EM1 presents a higher percentage (from 20

372 to 87%, with an average value of ~48%) below 300 cm than in the upper part of
373 the core (from 0 to 20%, with an average value of ~9%). In contrast, proportions
374 of EM2 are lower (from 0 to 54%, with an average value of ~29%) below 300 cm
375 than thereafter (from 16 to 79%, with an average value of ~58%).
376
377 3.3. Clay mineralogy
378
379 In core +59-07/293VE, smectite (15-97%) and illite (1.5-49%) are the dominant
380 clay minerals while chlorite (1.5-26%) and kaolinite (1-19%) are present in lesser
381 quantities (Figure 4). In general, illite, chlorite and kaolinite contents display
382 relatively similar distributions and are inversely correlated to smectite contents.
383 In the bottom section of the core (corresponding to the interval depth from 480 to
384 300 cm) the clay fraction is characterized by higher proportions of smectite (from
385 96 to 35%) and lower contents of illite (from 0.5 to 35%), chlorite (from 0.5 to
386 25%) and kaolinite (from 0.5 to 13%) when compared to the upper 300 cm.
387
388 In detail, between 485-410 cm, smectite content displays higher values (from
389 around 92 to 96%), before rapidly decreasing to 54% at 410 cm. This decrease in
390 smectite content is associated with an increase in illite and chlorite content, from
391 0.5 to 25% and 0.5 to 14%, respectively. In the core section from 390 cm to the
392 core top, the proportions of smectite continue to decrease rapidly from 54% to
393 35 % followed by a maximum of smectite (57%) around 315 cm. Thereafter the

smectite content decreases again around 300 cm, when the CWC appear, and decreases progressively from 35 to 10 % to the core top. This general decrease in smectite content in two steps with sharp transitions centred at 300 and 380 cm is associated with an increase in illite, chlorite and kaolinite contents.

4. Discussion

4.1. Potential diagenesis effect and the U/Th and ^{14}C age offset.

The comparison of U/Th and ^{14}C data sets reveals significant differences in the age depth relationships, particularly between 160-306 cm (Figures 2, 4 and Tables 1, 2) where differences in age of up to 2500-1500 years can be observed. A total of 12 paired U/Th and ^{14}C dates enable to estimate reservoir ages following similar approach as in previous studies (Frank et al., 2004; Douarin et al., 2015). Values range from 530 to >3000 years. Most of these reservoir age estimates are outside the natural range in the modern ocean and unexpected in surface waters so close to the area of formation of deep waters in the North Atlantic. In the section between 0-60 cm, above the interval with highly altered corals, three reservoir age estimates are between 530-1050 years, which is closer to the expected values, yet still significantly higher than recent estimates for the Holocene (Cage et al., 2006). We consider that our results attest of an of a diagenetic process that standard quality tests have failed to highlight. We further

hypothesise that there could be a relationship between the diagenesis processes and the reworked section of the core between 60-160cm, there are signs of dissolution and no well-preserved CWC fragments were found in this interval. We observe the largest age offsets between ^{14}C and U/Th ages in the core section 160-306 cm, which is just below the reworked layer (Figure 4).

Diagenetic processes in CWC environments have first been observed by Foubert et al., (2007) who proposed that the rapid accumulation (commonly between 50-100 cm/ka) rates in these environments was associated with an elevated oxidation of organic matter, which led to dissolution of aragonitic corals. Early diagenesis observed in sub-modern samples showed significant offsets between recent and older sections of the same coral fragment. However, these age offsets were of smaller magnitude and there was a coherent offset for ^{14}C ages (Pons-Branchu et al., 2005). More recently, other studies have described similar diagenetic processes (Pirlet et al., 2009, Raddatz et al., 2014). Pirlet et al., (2009) highlights the formation of gypsum associated to the oxidation of sedimentary sulphide minerals such as pyrite and the dissolution of carbonates. These authors explained the oxidation by a phase of increased bottom currents which caused erosion and enhanced inflow of oxidizing fluids into the mound sediments. We did not observe any presence of gypsum in our sediment core but further analyses would be required to exclude this possibility. However, both ^{14}C and U/Th dates were performed on the same sediment core as the one used by Pirlet et al., (2009) and

437 results do not show such large age offsets (Frank et al., 2009). It is thus unclear if
438 the oxidation of organic matter can cause modifications of the U/Th or ^{14}C ages.
439 Such a dissolution event may have occurred and could explain the absence of
440 well-preserved CWC in the interval 60-160 cm (Figure 4). However, there are no
441 signs of dissolution of the planktonic and benthic foraminifera which could
442 indicate that if there was dissolution, this would have affected mainly aragonite
443 and not calcite. This diagenetic imprint appears to have affected sediments up to
444 150 cm below the altered zone which was previously observed in the Challenger
445 mound (Pirlet et al., 2010). The absence of any alterations of the planktonic and
446 benthic foraminifera seems to indicate that this dissolution event may have
447 affected mainly aragonite and not calcite. Interestingly, several studies have
448 previously shown the presence of meter thick sediment layers with similar
449 characteristics and in similar settings. within sedimentary sequences similar to
450 that observed here between 60-160 cm (Figure 4) One of these sites is located
451 with abundant pyrite and dolomite on the Challenger Mound, a meter thick
452 sedimentary layer was enriched in pyrite and dolomite (Raddatz et al., 2014) .
453 Similarly, in a sediment core collected offshore Norway there was an absence of
454 well-preserved coral in a meter-long section (Raddatz et al., 2016). This later
455 study showed suggested evidence for changes in ocean pH which the authors
456 associated with post-glacial meltwater inputs. However, the timing of the
457 observed shift in ocean pH around is older, 5-6 ka BP (determined by U/Th dates)
458 when compared to results from our study site. Further analyses will be required

459 to fully explain the U/Th - ^{14}C offsets presented in this study and any links with
460 sedimentary processes we are observing.
461
462 4.2. Chronology of sedimentary deposits on the Wyville Thomson Ridge.
463
464 Our strategy has thus been to use the *G. bulloides* $\delta^{18}O$ profiles to build an
465 independent age model for this site based on the principles of isotope stratigraphy.
466 The stable isotope profile of vibrocore +59-07/293VE is compared to the *G.*
467 *bulloides* $\delta^{18}O$ profile of sediment core Na87-22 (Figure 5), which is a well-dated
468 sediment core located on the Rockall Plateau (Figure 1) (Waelbroeck et al., 2001).
469 The comparison of the two *G. bulloides* $\delta^{18}O$ profiles enabled to build an
470 independent age model based on matching of the isotope profiles (Figure 5). The
471 age depth relationship of this stratigraphic age model can be compared with the
472 U/Th and ^{14}C dates (Figure 5D). On Figure 5D, we consider the 60-160 cm zone
473 to be either a reworked altered mixed sedimentary layer. This first order
474 stratigraphic age model, built by matching *G. bulloides* $\delta^{18}O$ profiles, is based on
475 5 tie-points. T between the age core top 0 cm in modern or close to modern with
476 and is estimated age around 1.5 cal ka BP . This was the 'best fit' through both the
477 U/Th and ^{14}C dates. At 400 cm we estimated the age at around 13 cal ka BP based
478 on the match between the *G. bulloides* $\delta^{18}O$ profiles (Figure 5). The Finally, the
479 base of the sediment core is considered of glacial age (Figure 5). The accuracy of

480 the age model is variable downcore. The $\delta^{18}O$ transition observed between 300-
481 400 cm enables a more robust age estimate compared to the core top 0-300 cm
482 where a $\delta^{18}O$ plateau is observed. As a result we do not attempt to interpret
483 millennial-scale trends in our data at millennial-scale level, as done in previous
484 studies (e.g. Bonneau et al., 2018 , Colin et al., 2019).
485
486 Using this stratigraphic age model, the results of mineralogy and grain-size data
487 highlight three phases in sediment deposition, associated with significant shifts in
488 sedimentation rate. Firstly, glacial age sediment deposits between 400-495 cm
489 (Figure 5), with ages > 50-13 cal ka BP. Secondly, the deglacial sediments
490 accumulate between 306-400 cm (Figure 5), with ages between 13-9 cal ka BP.
491 Thirdly, Holocene sediments are deposited (the past 9 cal ka BP), corresponding
492 to the period of settlement of CWC, between 0-306 cm (Figure 5).
493
494 4.2.1. Glacial age sediments (40-13 cal ka BP)
495 The age of the base of the core, from 495-400 cm (Figure 5), is constrained by
496 four ^{14}C ages derived from marine bivalve fragments and foraminifera (from
497 22.91 to 40.66 cal ka BP and one age >50 cal ka BP). It dates back to the glacial
498 period. Sedimentation rates are low around 2-3 cm/ka with potential periods of
499 non-deposition or even erosion (Figure 5). During this period, the British ice sheet
500 extended northwards and covered large areas of the continental shelf (Clark et al.,
501 2010). The core site would have been shallower and closer to the shoreline and

potentially ice covered. The nearby continental ice sheets covered Scotland (Clark et al., 2010) and the Faroe Islands to the North (Figure 1). Episodes of ice-rafted debris deposits are possible during this period which would explain the presence of well-rounded large rock fragments and low content of biogenic fraction.

4.2.2. Deglacial sediments (13-9 cal ka BP)

The section between 400-306 cm corresponds to the end of the deglaciation/early Holocene and range approximately from 13 to 9 cal ka BP (Figure 5). Mean sedimentation rates increase to around 24 cm/ka. There are no *L. pertusa* fragments indicating that conditions were not yet suitable for CWC reef settlement during this interval. The age of this section of the core is mainly based on correlation of the *G. bulloides* $\delta^{18}O$ profile with core Na-87-22. Several ^{14}C dates are, however, coherent with this stratigraphic age model: a sample of a fossil bivalve at 308 cm (10.65 cal ka BP) and a *C. refulgens* ^{14}C sample at 300 cm (10.27 cal ka BP). However, one ^{14}C sample at 385 cm around 22 cal ka BP is too old and not coherent with the proposed age model. We suggest that this could be due to mixing or bioturbation of older sediments. This period correspond to the end of the Younger Dryas event and the following warm event at the end of this rapid climate cooling.

4.2.3. Settlement of CWC during the Holocene around 9 ka BP

523 The first well-preserved fossil fragments of *L. pertusa* appear at 306 cm with a
524 clear increase observed after 300 cm (Figure 4). Using the stratigraphic age model
525 the age of this transition is around 9 cal ka BP (Figure 5). The ages obtained from
526 U/Th and ^{14}C on fossil coral samples during this interval differ by several
527 thousand years (Figure 4 and 5). The ages derived from the first dated samples at
528 306 cm are much younger, at around 5.2-5.6 cal ka BP for U/Th dates, whereas
529 the *L. pertusa* ^{14}C dates are within error of this age estimate around 8.3 cal ka BP.
530 As a result estimated mean sedimentation rates are variable (70-34 cm/ka) and
531 depend on which age model or which data set is used, particularly during the 9-4
532 cal ka BP interval (Figure 2). In the top 60 cm, both U/Th and ^{14}C show a drop in
533 sedimentation rate after 4-5 cal ka BP to around 7 cm/ka (Figure 5).
534 The important difference between the ^{14}C and U/Th ages raises some uncertainty
535 on the ages obtained in this section of the core. The chronology proposed based
536 on stable isotope stratigraphy provides an age around 9 cal ka BP for the
537 settlement of the CWC reef. This age is, however, supported by ^{14}C dates 1- *L.*
538 *pertusa* ^{14}C date at 306 cm of 8.4 cal ka BP, 2- the *C. refulgens* ^{14}C date at 300
539 cm around 10.3 cal ka BP and 3- the *Venus casima* ^{14}C date at 308 cm is around
540 10.6 cal ka BP (Table 1). Furthermore, in a nearby site, but in a deeper setting at
541 around 900 m water depth, a slightly older age has been found for the first
542 occurrence of *L. pertusa* at around 10.3 cal ka BP (Victoreo et al., 2016). We
543 consider that these ^{14}C ages are consistent and support the stratigraphic age model
544 proposed here.

545

546 4.3. Transition from glacial to deglaciation on the Wyville Thomson Ridge

547

548 The glacial age sediment deposits are characterised by high values of mean grain
549 size (Figure 5). Grain-size distributions of the siliciclastic fraction can be used to
550 infer the hydrographic conditions at the time of deposition (e.g. Ballini et al.,
551 2006; Prins et al., 2002) and have already been used to establish past current
552 intensity and the presence of IRD deposits in CWC mound records (e.g. Pirlet et
553 al., 2011; Thierens et al., 2012). The grain-size distribution indicates strong
554 variations in agreement with lithological description and glacial and interglacial
555 changes. Glacial age sediments show a poorly-sorted bimodal grain-size
556 distribution associated with sediments enriched in coarse (>150 m) lithic particles
557 which points towards ice-rafting as a likely transport and sedimentation
558 mechanism (Figure 3). The presence of dropstones (rock fragments up to several
559 centimeters) below 400 cm, confirm that these sediments are of glaciomarine
560 origin.

561

562 The grain-size distribution of EM3 characterizes poorly sorted sediments,
563 enriched in the coarser size fractions of up to 800 m, which can be attributed to
564 sediments transported by icebergs (e.g. Prins et al., 2002; Pirlet et al., 2011;
565 Thierens et al., 2012) (Figure 3). EM3 dominates the glacial period indicating a
566 predominance of coarse sediments transported by icebergs most probably from

567 the BIS in agreement with the maximum extent of the continental ice sheets
568 during this period (Figure 1) (Golledge et al., 2008; Clark et al., 2010). In addition,
569 such poorly sorted grain-size distribution during glacial times suggests that the
570 coastal current was sluggish in the studied area and was unable to sort coarse
571 glaciomarine deposits as it was also observed for glacial sediments of CWC
572 mounds of the Porcupine Seabight (Pirlet et al., 2011).
573
574 These coarse glacial sediments are associated with high content of smectite that
575 reach up to 96%. Clay mineral assemblages of the high latitude of the North
576 Atlantic can reveal information on the palaeo-environmental conditions that
577 governed continental weathering processes on adjacent landmasses and/or
578 sedimentary sources (e.g. Chamley, 1989; Fagel et al., 1996; Bout-Roumazeilles
579 et al., 1997; Ballini et al., 2006; Pirlet et al., 2011). Sediment distributions and
580 sources in the NE Atlantic have been established in several previous studies
581 (Biscaye, 1965; Latouche, 1975; Windom, 1976; Grousset et al., 1982; Grousset
582 and Para, 1982; Latouche and Para, 1976; Pirlet et al., 2011; Thierens et al., 2012).
583 Clay mineralogical composition of surface sediments of the NE Atlantic (between
584 the Faroe and Shetland Islands and the northern margin of North Scotland) is
585 mainly controlled by the petrology of the eroded source area. The clay fraction of
586 sediments north of the Wyville Thomson Ridge and south of Iceland is
587 characterized by abundant smectites (50-100%) compared to illite (0-30%)
588 deriving from the weathering of basaltic rocks from the Iceland and the Faroe-

589 Shetland ridge area (e.g. Latouche, 1975; Grousset et al., 1982). The weathering
590 of these volcanic rocks provides large quantities of smectite transported
591 southward by oceanic currents and smectite composes up to 90% of the clay
592 fraction in the sediments surrounding the Iceland and Faroe Islands (Grousset et
593 al., 1982) and on the pathway of deep-current circulating along this volcanic
594 province (e.g. Iceland Scotland Overflow Water; Fagel et al., 1996 ; Ballini et al.,
595 2006 ; Fagel et al., 2006). On the contrary, the clay fraction in sediments from the
596 Scottish and Irish continental shelves has high content in illite (> 50% illite)
597 (Latouche, 1975; Windom et al., 1976) and low smectite concentrations (<20 %)
598 sourced from physical erosion of soils of northern Europe, which developed on
599 crustal rock formations under cold and intermediate climates.
600
601 Consequently, the smectite/illite (Sm/I) ratio reported in Figure 5 can be used
602 here to track clay minerals deriving from the weathering of the northern Iceland-
603 Scotland Ridge basalts (smectite) and the more local sources of clay derived from
604 soils developed on crustal rock formations from North Scotland which are
605 transported via river flow and then coastal currents. Similar studies have used this
606 proxy to separate the Icelandic source of the clay fraction from sediments in the
607 North Atlantic at different times scales (e.g. Fagel et al., 1996; Bout-Roumazeilles
608 et al., 1997; Ballini et al., 2006 ; Fagel et al., 2006). In core +59-07/293VE, this
609 mineralogical ratio ranges from 0.2 to 33, with last deglacial sediment values

610 being higher than those for the late Holocene (Figure 5), and is characterized by
611 two abrupt decrease around 13 and 9 ka BP.
612
613 The high concentration of smectite in the glacial deposits at the study site implies
614 that clay minerals are mainly sourced from a northern volcanic source such as the
615 Iceland-Scotland Ridge basalts (Ziska and Varming et al 2008). This contrasts
616 significantly with the grain-size data which imply a local source of ice-rafted
617 material most probably from the BIS. A possible explanation is that the ice-rafted
618 material transported small quantities of the illite and chlorite and mainly coarser
619 material as shown by the high values of EM3. This can be explained by a lack of
620 soil produced over the ice covered Scottish continent during glacial periods. The
621 fine sized clay material would be primarily produced during warm interglacial
622 periods and would be rapidly exported during the initial glacial phase in
623 agreement with results obtained by Pirlet et al. (2011) and Thierens et al. (2012)
624 in the Porcupine Seabight. The high values of smectite also imply significant
625 modifications of ocean circulation with possible southward flow of surface waters
626 during glacial periods. This is in agreement with a map of reconstructed surface
627 currents for this area obtained by Sarnthein et al. (1995) indicating that surface
628 currents were flowing southward during the glacial and northward flowing during
629 the Holocene.
630

631 At around 13 cal ka BP, there is a sharp transition marked by a reduction of
632 smectite whereas the mean grain size does not change significantly until around
633 9 cal ka BP (Figure 5). The proportion of EM3 remains high and sediments are
634 still poorly sorted, which means that currents in the study area remained sluggish
635 during this period. The opposing signals observed in the clay mineralogy and
636 grain-size data imply sources and transports of different sedimentary size
637 fractions as described during the glacial periods. During the interval 9-13 cal ka
638 BP, towards the end of the deglaciation, smectite concentrations remain high
639 around 30-40% corresponding to a mixed volcanic northern source and
640 sedimentary material from a southern source. This period 13-9 cal ka BP thus
641 marks a shift in oceanic currents occurs which is at the study site at the end of the
642 deglaciation, and associated with the initiation of shelf currents (SCC and SEC),
643 which flow northwards along the west coast of Scotland and transport the
644 sedimentary material to the study area via (Simson and Hill 1986). In addition, at
645 9-9 13 cal ka BP, the northern regions of the Scottish mainland were became
646 progressively ice free (Golledge et al., 2008). The soils that developed during the
647 warmer climatic conditions of the early Holocene Such a configuration would
648 have permitted the production and transport by river runoff of a larger quantities
649 of illite and chlorite from soils that developed during the warmer climatic
650 conditions of the early Holocene.
651

652 4.4. Cold water reef settlement and sedimentary environment during the early
653 Holocene
654
655 The final transition in sediment properties occurs during the early Holocene
656 around 9 cal ka BP when a second significant change in clay mineralogy is
657 associated with a change in mean grain size and a significant increase in
658 sedimentation rates (Figure 5). This transition is coeval with the CWC reef
659 settlement at the study site. There is a strong reduction of the smectite (around
660 35%, decreasing thereafter to 15%), and a significant increase of both illite (35%,
661 increasing thereafter to 50%) and chlorite (25%) (Figure 5) . These observations
662 attest of a reduction of the northern-sourced smectite and an increase of Scottish-
663 sourced illite and chlorite. The grain-size data shows a sharp reduction of EM3
664 and an increase of EM2 which implies more energetic bottom-water flow able to
665 sort sediment and the source of the clay sized fraction. We interpret this data as
666 evidence for a sudden change in energy and possibly direction of bottom-water
667 currents around 9 cal ka BP, which we interpret as reflecting an increase in
668 southern sourced oceanic currents (mainly the SEC and the SCC) that bring clay
669 minerals from the coastal areas and the continental shelves surrounding the
670 Scottish mainland. At 9 cal ka BP, the northern regions of the Scottish mainland
671 are ice free (Golledge et al., 2008). Such a configuration would have permitted
672 the production and transport by river runoff of a larger quantity of illite and
673 chlorite from soils .

674

675 The meltwater produced by the final decay of the large continental ice sheets has
676 been shown to affect ocean circulation patterns in the North Atlantic, reducing the
677 salinity and the vigour of the North Atlantic Current (and AMOC) until around 8
678 cal ka BP (Thornalley et al., 2013; Mjell et al., 2013; Hoogakker et al., 2011;
679 Gherardi et al., 2009; Kissel et al., 2013). These changes in salinity are known to
680 have affected the strength of the NAC, which could also have affected the flow
681 regimes of the SCC and SEC in this area. Consequently, the settlement of CWC
682 at 9 cal ka BP seems related to a major shift in North Atlantic circulation patterns.
683 Sortable silt records form sediment cores located south of Iceland show a gradual
684 increase in deep-water circulation observed around 8-6 cal ka BP on the Scotland
685 Iceland overflow water (Mjell et al., 2013; Hoogakker et al., 2011; Thornalley et
686 al., 2013) associated to an intensification and eastward extension of the sub-polar
687 gyre (e.g. Thornalley et al., et al., 2009; Colin et al., in press2019). This transition
688 centred around 8 cal ka BP has been associated with the final decay of the northern
689 hemisphere ice sheets.

690

691 5. Conclusions

692

693 Results from a vibrocore located on the Wyville Thomson Ridge North of the
694 Scottish continental shelf at 300 m water depth enables to estimate the age of the
695 onset of cold water coral reef growth in this area. Multiple U/Th and ^{14}C dates

696 were derived from fossil *Lophelia pertusa*, marine bivalves and foraminifera. The
697 oldest cold water coral, L. pertusa, fragments dated by ^{14}C and U/Th dates are 8.4
698 and 7.9 cal ka BP, respectively. However, we observe significant and unexplained
699 differences between paired samples of ^{14}C and U/Th dates, which appear to be
700 affected by a diagenetic effect which we do not yet fully explain. We thus derived
701 an independent age model based on isotope stratigraphy using profiles of $\delta^{18}O$
702 derived from planktonic species *G. bulloides*. The reconstructed age model
703 enables to provide an independent estimate of the date the onset of reef growth to
704 around 9 cal ka BP, which is coherent with the ^{14}C dates of the oldest CWC
705 sample.
706
707 Grain size and clay mineralogy provide information about the evolution of the
708 flow patterns and direction of water currents in this area. These records show 2
709 marked transitions at around 13 and 9 cal ka BP. We thus identify 3 periods
710 characterised by different clay mineralogy and grain size: a glacial period (prior
711 de 13ka BP), an end of deglaciation (13-9 cal ka BP) and a Holocene section (9
712 to modern cal ka BP).
713
714 The first transition at 13 cal ka BP, is characterized by a shift of smectite-rich,
715 poorly sorted sediments to a mixed clay mineralogy of smectites and illites. This
716 transition marks the end of the glacial period, when clay mineralogy was
717 dominated by smectite (75 to 96%) to the deglaciation when the % smectite

718 reduces to 50%. Such mineralogical changes that can be observed between 13 and
719 9 cal ka BP indicate large variations of sediment sources from the volcanic
720 province of the Iceland-Faroe Ridge (smectite) to a crustal province of the north
721 of Scotland (illite and chlorite). This period is also associated with a strong
722 decrease of the siliciclastic grain size. Sediments become better sorted which
723 reflects an increase of bottom-current velocity. There is a decrease of IRD
724 deposits linked to the retreat of the northern glacial ice sheet and.
725
726 The second transition is clearly associated with the appearance of CWC, *Lophelia*
727 *pertusa*, at this site. At around 9 cal ka BP, illite and chlorite increase to 49% and
728 25%, respectively, and the mean grain size reduces and the sediments become
729 well sorted. Our results show that the onset of CWC growth on the Wyville
730 Thomson Ridge occurred around 9 cal ka BP and was associated with changes in
731 ocean circulation patterns in this area. This age corresponds to the final phases of
732 the post glacial sea level rise and final melting of continental ice sheets. The clay
733 mineralogy enables to identify a sudden changes in the flow patterns of bottom-
734 water currents that induces favourable sedimentological and hydrological
735 conditions for coral growth.
736
737 Acknowledgements
738 We would like thank the British Geological Survey for granting access to
739 sediment core material. The research leading to this study has received funding

740 from the French National Research Agency "Investissement d'Avenir"
741 (n¬∞ANR-10-LABX-0018), the HAMOC project ANR-13-BS06-0003, and the
742 Region Pays de Loire (New Research Group initiative). We thank the Andres
743 Rüggeberg and one anonymous reviewer for their constructive comments which
744 helped improve the quality of the paper. We also thank Marc de Batist for his
745 editorial handling of the manuscript.

746

747

748

749 References:

750

751 Ballini, M., Kissel, C., Colin, C., Richter, T., Dokken T. (2006) Deep-water mass
752 source and dynamic associated to rapid climatic variations during the last glacial
753 stage in North Atlantic: a multi-proxy investigation of the detrital fraction of deep-
754 sea sediments, Geochemistry, Geophysics and Geosystems, 7, Q02N01,
755 doi:10.1029/2005GC001070.

756 Baltzer A., Bates R., Mokeddem Z., Clet-Pellerin M., Walter-Simonnet A-V,
757 Bonnot-Courtois C. & Austin W.N. (2010) Using seismic facies and pollen
758 analyses to evaluate climatically driven change in a Scottish sea loch (fjord) over
759 the last 20 ka. in Howe, J. A., Austin, W. E. N., Forwick, M. & Paetzel, M. (eds)
760 Fjord Systems and Archives. Geological Society, London, Special Publications,
761 344, 357-371

762 Biscaye, P.E. (1965) Mineralogy and sedimentation of the Recent Deep-Sea Clay
763 in the Atlantic Ocean and Adjacent Seas and Oceans, Geol. Soc. Am. Bull. 76.
764 Bonneau L., Colin C., Pons-Branchu E., Mienis F., Tisnerat-Laborde N., Blamart
765 D., Elliot M., Collart T., Frank N., Foliot L., Douville E. (2018) Imprint of
766 Holocene climate variability on cold-water coral reef growth at the SW Rockall
767 Trough margin, NE Atlantic. Geochemistry, Geophysics, Geosystems.
768 Bout-Roumazeilles, V. et al. (1997): Latitudinal control of astronomical forcing
769 parameters on the high-resolution clay mineral distribution in the 45¬∞-60¬∞ N
770 range in the North Atlantic Ocean during the past 300,000 years.
771 Paleoceanography, 12(5), 671-686
772 Chamley, H. (1989) Clay Sedimentology, Springer-Verlag, New-York. 623 pp.
773 Cheng, H., Lawrence Edwards, R., Shen, C.-C., Polyak, V. J., Asmerom, Y.,
774 Woodhead, J. D., Hellstrom, J., Wang, Y., Kong, X., Spötl, C., Wang, X., &
775 Calvin Alexander, E. (2013), Improvements in 230Th dating, 230Th and 234U
776 half-life values, and U-Th isotopic measurements by multi-collector inductively
777 coupled plasma mass spectrometry, Earth Planet. Sci. Lett., 371-372, 82-91
778 Clark C. D., Hughes A.L.C., Greenwood S.L., Jordan C., Sejrup H.P., (2012)
779 Pattern and timing of retreat of the last British-Irish Ice Sheet, Quaternary Science
780 Reviews, 44, 112-146.
781 Christophe Colin, Nadine Tisnérat-Laborde, Furu Mienis, Tim Collart, Edwige
782 Pons-Branchu, Quentin Dubois-Dauphin, Norbert Frank, Arnaud Dapoigny,
783 Mohamed Ayache, Didier Swingedouw, Jean-Claude Dutay, Frédérique Eynaud,

784 Maxime Debret, Dominique Blamart, Eric Douville (2019). Millennial-scale
785 variations of the Holocene North Atlantic mid-depth gyre inferred from
786 radiocarbon and neodymium isotopes in cold water corals, Quaternary Science
787 Reviews, 211, 93-106,
788 Davies, A.J., Wisshak, M., Orr, J.C., & Roberts, J.M. (2008), Predicting suitable
789 habitat for the cold-water coral *Lophelia pertusa* (Scleractinia). Deep Sea Res.,
790 Part I, 55, 1048-1062.
791 Quentin Dubois-Dauphin, Christophe Colin, Mary Elliot, Arnaud Dapoigny, Eric
792 Douville, (2019) Holocene shifts in sub-surface water circulation of the North-
793 East Atlantic inferred from Nd isotopic composition in cold-water corals, Marine
794 Geology, 410, 135-145.
795 De Haas, H., Mienis, F., Frank, N., Richter, T.O., Steinacher, R., de Stigter, H.,
796 van der Land, C., & van Weering, T.C.E. (2009), Morphology and sedimentology
797 of (clustered) cold-water coral mounds at the south Rockall Trough margins, NE
798 Atlantic Ocean. Facies, 55, 1-26.
799 De Mol, L., Van Rooij, D., Pirlet, H., Greinert, J., Frank, N., Quemmerais, F.,
800 Henriet, J.P., (2011). Cold-water coral habitats in the Penmarc'h and Guilvinec
801 Canyons (Bay of Biscay): Deep-water versus shallow-water settings. Marine
802 Geology, 282(1-2), 40-52.
803 Dobigeon, N., Moussaoui, S., Tourneret, J.-Y., Carteret, C., (2009). Bayesian
804 separation of spectral sources under non-negativity and full additivity constraints,
805 Signal Processing, 89, 2657-2669.

806 Dorschel, B., Hebbeln, D., Rüggeberg, A., Dullo, C., & Freiwald, A. (2005),
807 Growth and erosion of a cold-water coral covered carbonate mound in the
808 Northeast Atlantic during the Late Pleistocene and Holocene. Earth and Planetary
809 Science Letters, 233, 33-44.
810 Douarin, M., Elliot, M., Noble, S.R., Sinclair, D., Henry, L.-A., Long, D.,
811 Moreton, S.G., & Roberts J.M. (2013), Growth of north-east Atlantic cold water
812 coral reefs and mounds during the Holocene: A high resolution U-series and ^{14}C
813 chronology, Earth Planet. Sci. Lett., 375, 176-187.
814 Douarin, M., M. Elliot, D. Sinclair, S.G. Moreton, S.R. Noble, D. Long, and J.M.
815 Roberts (2015) "North Atlantic Ecosystem Sensitivity to Shifts in Meridional
816 Overturning Circulation" Geophys. Res. Lett., 42, doi:10.1002/2015GL065999,
817 2015.
818 Douville, E., Sall√©, E., Frank, N., Eisele, M., Pons-Branchu, E., & Ayrault, S.
819 (2010), Rapid and precise 230Th/U dating of ancient carbonates using Inductively
820 Coupled Plasma - Quadrupole Mass Spectrometry. Chem. Geol., 272, 1-11.
821 Dons C (1944) Norges korallrev. K Nor Videns Selsk Forh 16: 37-82
822 Dullo, C., Fl√∂gel, S., & Rüggeberg, A. (2008), Cold-water coral growth in
823 relation to the hydrography of the Celtic and Nordic European continental margin.
824 Marine Ecology Progress Series, 371, 165-176.
825 Eisele, Marku.s, & Frank, Norbert F., & Wienberg, Claudia C.,& Hebbeln, Dierk
826 D., & L√≥pez Correa, Matthias M., & Douville, Eric E. and& Freiwald, Andre.
827 (2011). Productivity controlled cold-water coral growth periods during the last

828 glacial off Mauritania. Marine Geology. 280. 143-149.
829 10.1016/j.margeo.2010.12.007.
830 Ellett, D.J., (1979). Some oceanographic features of Hebridean waters.
831 Proceedings of the Royal Society of Edinburgh, vol. 77B, pp. 61-74.
832 Ellett, D.J., & Edwards, A. (1983). Oceanography and inshore hydrography of the
833 Inner Hebrides. Proceedings of the Royal Society of Edinburgh. Section B.
834 Biological Sciences. 83. 10.1017/S0269727000013385.
835 Ellett, D.J., Edwards, A., & Bowers, R. (1986), The hydrography of the Rockall
836 Channel - An overview. Proc. R. Soc. Edinburgh, Sect. B, Biol. Sci., 88, 61-81.
837 Fagel, N., Robert, C., and Hillaire-Marcel, C. (1996), Clay mineral signature of
838 the NW Atlantic Boundary Undercurrent, Marine Geology, 130, 19-28.
839 Findlay, H.S., Hennige, S.J., Wicks, L.C., Navas, J.M., Woodward, E.M.S., and&
840 Roberts, J.M. (2014), Fine-scale nutrient and carbonate system dynamics around
841 cold-water coral reefs in the northeast Atlantic. Scientific Reports, 4, DOI:
842 10.1038/srep03671.
843 Foubert, A., Van Rooij, D., Blamart, D. and Henriet, J.-P. (2007) X-ray imagery
844 and physical core logging as a proxy of the content sediment cores in cold-water
845 coral mound provinces: a case study from Porcupine Seabight, SW of Ireland. Int.
846 J. Earth Sci. (Geol. Rundsch.), 96, 141-158.
847 Frank, N., Paterne, M., Ayliffe, L., van Weering, T., Henriet, J.-P., and Blamart,
848 D., (2004). Eastern North Atlantic deep-sea corals: tracing upper intermediate
849 water ^{14}C during the Holocene. Earth Planet. Sci. Lett. 219, 297-309.

850 Frank, N., Ricard, E., Paquet, A., van der Land, C., Colin, C., Blamart, D.,
851 Foubert, A., Van Rooij, D., Henriet, J.-P., de Haas, H., and& van Weering, T.
852 (2009), The Holocene occurrence of cold water corals in the NE Atlantic:
853 implications for coral carbonate mound evolution. Marine Geology, 266, 129-
854 142.
855 Frank, N., Freiwald A., Matthias López Correa M., Wienberg C., Eisele M.,
856 Hebbeln D., Van Rooij D., Henriet J.-P. Colin C., van Weering T., de Haas H.,
857 Buhl-Mortensen P., Murray Roberts J., De Mol B., Douville E., Blamart D., and&
858 Hatt√© C. (2011), Northeastern Atlantic cold-water coral reefs and climate.
859 Geology, 39, 743-746.
860 Frederiksen, R., A. Jensen, and H. Westerberg. (1992). The distribution of the
861 scleractinian coral *Lophelia pertusa* around the Faeroe islands and the relation to
862 internal tidal mixing. Sarsia 77:157-171.
863 Freiwald, A. (2002), Reef-forming cold-water corals, in Ocean Margin Systems,
864 edited by G. Wefer et al., pp. 365-385 , Springer, Berlin.
865 Freiwald, A., Fosså, J.H., Grehan, A., Koslow, T., and Roberts, J.M. (2004), Cold-
866 water coral reefs: out of sight - no longer out of mind. Biodiversity Series 22.
867 Cambridge (UK): UNEP World Conservation Monitoring Centre. 86 pp.
868 Freiwald, A., Rogers, A., Hall-Spencer, J., Guinotte, J.M., Davies, A.J., Yesson,
869 C., Martin, C.S., and Weatherdon, L.V. (2017), Global distribution of cold-water
870 corals (version 3.0). Second update to the dataset in Freiwald et al. (2004) by

871 UNEP-WCMC, in collaboration with Andre Freiwald and John Guinotte.
872 Cambridge (UK): UNEP World Conservation Monitoring Centre.
873 Gherardi, J.M., Labeyrie, L., Nave, S., Francois, R., McManus, J.F. and, Cortijo,
874 E., (2009). Glacial-interglacial circulation changes inferred from Pa-231/Th-230
875 sedimentary record in the North Atlantic region. Paleoceanography 24.
876 Grousset, F., Latouche, C., and Parra, M. (1982). Late Quaternary sedimentation
877 between the Gibbs fracture and the Greenland basin : mineralogical and
878 geochemical data. Mar. Geo., 47, 303-330.
879 Grousset, F., Parra, M. (1982) Contribution of mineralogical and geochemical
880 data to the study of northeast Atlantic deep quaternary sediments : trace-elements
881 as bottom current indicators, Sedim. Geol. 31, 49-61
882 Golledge N.R. et al. (2008) High-resolution numerical simulation of Younger
883 Dryas glaciation in Scotland. Quaternary Science Reviews 27 (2008) 888-904
884 Hennige S.J., Wicks L.C., Kamenos N.A., Perna G., Findlay H.S., Roberts J.M.
885 (2015) Hidden impacts of ocean acidificationto live and dead coral framework.
886 Proc. R. Soc. B 282
887 Henriet J.P., De Mol B., Pillen S., Vanneste M. and others (1998) Gas hydrate
888 crystals may help build reefs. Nature 391: 648-649
889 Henry, L.-A., Frank, N., Hebbeln, D., Wienberg, C., Robinson, L., de Flierdt, T.
890 Van, Dahl, M., Douarin, M., Morrison, C.L., Correa, M.L., Rogers, A.D.,
891 Ruckelshausen, M., Roberts, J.M., (2014). Global ocean conveyor lowers
892 extinction risk in the deep sea. Deep-Sea Res. I Oceanogr. Res. Pap. 88, 8-16.

893 Hill A.E. and Mitchelson-Jacob E.G. (1993) Observations of a poleward-flowing
894 saline core on the continental slope west of Scotland. Deep Sea Research42 (7),
895 1521-1527.
896 Holliday, N.P., Pollard, R.T., Read, J.F., and Leach, H. (2000), Water mass
897 properties and fluxes in the Rockall Trough, 1975 to 1998. Deep-Sea Research,
898 47, 1303-1332.
899 Hoogakker, B.A.A., Chapman, M.R., McCave, I.N., Hillaire-Marcel, C., Ellison,
900 C.R.W., Hall, I.R. and Telford, R.J., 2011. Dynamics of North Atlantic Deep
901 Water masses during the Holocene. Paleoceanography, 26, 1-10.
902 Howe, J.A., Dove, D., Bradwell, T. and Gafeira, J., (2012). Submarine
903 geomorphology and glacial history of the Sea of the Hebrides, UK. Mar. Geol.
904 315-318, 64-76.
905 Inall M., Gillibrand P., Griffiths, C., MacDougal, N., Blackwell, K. (2009) On the
906 oceanographic variability of the North-West European Shelf to the West of
907 Scotland. Journal of Marine Systems 77 (2009) 210-226.
908 Jaffey, A.H., Flynn, K.F., Glendenin, L.E., Bentley, W.C., & Essling, A.M.
909 (1971), Precision measurements of half-lives and specific activities of 235U and
910 238U. Phys. Rev. C, 4(5), 1889-1906.
911 Kenyon, N.H., Akhmetzhanov, A.M., Wheeler, A.J., Van Weering, T.C.E., De
912 Haas, H., & Ivanov, K. (2003), Giant carbonate mud mounds in the southern
913 Rockall Trough. Marine Geology, 195, 5-30.

914 Kissel, C. et al. (2013) Variations in the strength of the North Atlantic bottom
915 water during Holocene Earth and Planetary Science Letters 369-370, 248-259
916 Lambeck, K.; Rouby, H.; Purcell, A.; Sun, Y.; Sambridge, M. Sea level and ice
917 volume since the glacial maximum Proceedings of the National Academy of
918 Sciences Oct 2014, 111 (43) 15296-15303;
919 Latouche, C. (1975) Les min√©raux argileux des sediments actuels de
920 l'Atlantique Nord Oriental et du Sud de la mer de Norv√©ge. Proceeding of the
921 Interntional Clay Conference.
922 Latouche, C., Parra, M. (1976) Mineralogie et geochimie des sediments
923 quaternaires de l'Ocean Atlantique nord-oriental (Mer de Norv√®ge - golfe de
924 Gascogne) - essais d'interpr√©tations sedimentologiques, Mar. Geol. 22, 33-69.
925 Le Danois E. (1948) La profondeur de la mer. Payot, Paris
926 Long, D., Roberts, J.M., Gillespie, E.J., (1999). Occurrences of *Lophelia pertusa*
927 on the Atlantic margin. British Geological Survey Report WB/99/24, Edinburgh,
928 23pp and appendices.
929 Lopez-Correa, M., Montagna, P., Joseph, N., Ruggeberg, A., Fietzke, J., Flogel,
930 S., Dorschel, B., Goldstein, S. L., Wheeler, A., & Freiwald, A. (2012), Preboreal
931 onset of cold-water coral growth beyond the Arctic Circle revealed by coupled
932 radiocarbon and U-series dating and neodymium isotopes. Quaternary Science
933 Reviews, 34, 24-43.
934 Ludwig, K.R., & Titterington, D.M. (1994), Calculation of 230Th/U isochrons,
935 ages, and errors, Geochim. Cosmochim. Acta, 58(22), 5031-5042.

936 Lutringer, A. (2003), Reconstitution de la variabilité des eaux intermédiaires par
937 l'étude de la géochimie des coraux profonds. PhD Thesis, University of Paris XI,
938 234p.
939 Marsh R. et al.: Large-scale forcing of the European Slope Current and associated
940 inflows to the North Sea Ocean Sci., 13, 315-335, 2017
941 Matos et al. (2017) Coral mound development at the Campeche cold-water coral
942 province, southern Gulf of Mexico: Implications of Antarctic Intermediate Water
943 increased influence during interglacials Cape Lookout Cape Lookout
944 Matos, L., Mienis, F., Wienberg, C., Frank, N., Kwiatkowski, C., Groeneveld, J.,
945 Thil, F., Abrantes, F., Cunha, M.R., Hebbeln, D., (2015). Interglacial occurrence
946 of cold-water corals off Cape Lookout (NW Atlantic): first evidence of the Gulf
947 Stream influence. Deep-Sea Res. I Oceanogr. Res. Pap. 105, 158-170.
948 McCartney M.S., Mauritzen, C. (2001) On the origin of the warm inflow to the
949 Nordic Seas Progress in Oceanography 51, 125-214
950 McCulloch M., Taviani M., Montagna P., Lopez-Correa M., Remia A., Mortimer,
951 G. (2010). Proliferation and demise of deep-sea corals in the Mediterranean
952 during the Younger Dryas. Earth and Planetary Science Letters. 298. 143-152.
953 10.1016/j.epsl.2010.07.036.
954 Mjell T., Ninnemann U., Eldevik T., Kleiven H (2015). Holocene multidecadal-
955 to millennial-scale variations in Iceland-Scotland overflow and their relationship
956 to climate. Paleoceanography. 30. n/a-n/a. 10.1002/2014PA002737.

957 Mokeddem Z., Baltzer A., Goubert E & Clet-Pellerin M. (2010) A multiproxy
958 palaeoenvironmental reconstruction of Loch Sunart (NW Scotland) since the Last
959 Glacial Maximum in Howe, J. A., Austin, W. E. N., Forwick, M. & Paetzel, M.
960 (eds) Fjord Systems and Archives. Geological Society, London, Special
961 Publications, 344, 343-355.
962 Masson, D.G., Bett, B.J., Billett, D.S.M., Jacobs, C.L., Wheeler, A.J., & Wynn
963 R.B. (2003), The origin of deep-water, coral-topped mounds in the northern
964 Rockall Trough, Northeast Atlantic. Marine Geology, 194, 159-180.
965 Mienis, F., De Stigter, H.C., White, M., Duineveld, G., De Haas, H., & Van
966 Weering, T.C.E. (2007), Hydrodynamic controls on cold-water coral growth and
967 carbonate-mound development at the SW and SE Rockall Trough Margin, NE
968 Atlantic Ocean. Deep-Sea Res. I, 54, 1655-1674.
969 Mienis, F., van der Land, C., de Stigter, H.C., van de Vorstenbosch, M., de Haas,
970 H., Richter, T., & van Weering T.C.E. (2009), Sediment accumulation on a cold-
971 water carbonate mound at the Southwest Rockall Trough margin. Marine
972 Geology, 265, 40-50.
973 Moussaoui, S., Brie, D., Mohammad-Djafari, A., Carteret, C., 2006. Separation
974 of Non-Negative Mixture of Non-Negative Sources Using a Bayesian Approach
975 and MCMC Sampling, IEEE Transactions on Signal Processing, 54, 4133-4145.
976 Pirlet, H., Colin, C., Thierens, M., Latruwe, K., Van Rooij, D., Foubert, A., Frank,
977 N., Blamart, D., Huvenne, V.A.I., Swennen, R., Vanhaecke, F., & Henriet, J.-P.

978 (2011), The importance of the terrigenous fraction within a cold-water coral
979 mound: A case study. Marine Geology, 282, 13-25.
980 Pirlet H., LM Wehrmann, B Brunner, N Frank, J Dewanckele, D Van Rooij, A.
981 Foubert, R. Swennen, L. Naudts, M. Boone, V. Cnudde, J.,ÄêP. Henriet (2009)
982 Diagenetic formation of gypsum and dolomite in a cold,Äêwater coral mound in
983 the Porcupine Seabight, off Ireland. Sedimentology 57 (3), 786-805
984 Pollard, R. T., J. F. Read, and N. P. Holliday (2004) Pollard Water masses and
985 circulation pathways through the Iceland Basin during Vivaldi 1996. Journal of
986 Geophysical Research, 109, C04004
987 Pons-Branchu, E., Douville, E., Roy-Barman, M., Dumont, E., Branchu, P., Thil,
988 F., Frank, N., Bordier, L., & Borst, W. (2014), A geochemical perspective on
989 Parisian urban history based on U-Th dating, laminae counting and yttrium and
990 REE concentrations of recent carbonates in underground aqueducts. Quat.
991 Geochronol., 24, 44-53.
992 Pons-Branchu, E., Hillaire-Marcel, C., Ghaleb, B., Deschamps, P., & Sinclair, D.
993 (2005), Early diagenesis impact on precise U-series dating of Deep-Sea corals.
994 Example of a 100-200 years old *Lophelia pertusa* sample from NE Atlantic.
995 Geochimica et Cosmochimica Acta, 69 (20), 4865-4879.
996 Prins, M. A., L. M. Bouwer, C. J. Beets, S. R. Troelstra, G. J. Weltje, R. W. Kruk,
997 A. Kuijpers, Vroon, P. Z., (2002), Ocean circulation and iceberg discharge in the
998 glacial North Atlantic: Inferences from unmixing of sediment size distributions,
999 Geology, 30(6), 555-558.

1000 Raddatz, J., Liebetrau, V., Trotter, J., Rüggeberg, A., Flogel, S., Dullo, W.,ÄêC.,
1001 Eisenhauer, A., Voigt, S., and McCulloch, M. (2016), Environmental constraints
1002 on Holocene cold-water coral reef growth off Norway: Insights from a multiproxy
1003 approach, Paleoceanography, 31, 1350-1367.
1004 Raddatz, J., Rüggeberg, A., Liebetrau, V., Foubert, A., Hathorne, E.C., Fietzke,
1005 J., Eisenhauer, A., & Dullo, W.-C. (2014), Environmental boundary conditions of
1006 cold-water coral mound growth over the last 3 million years in the Porcupine
1007 Seabight, Northeast Atlantic. Deep Sea Research Part II: Topical Studies in
1008 Oceanography, 99, 227-236.
1009 Robinson, L. F., Adkins, J. F., Frank, N., Gagnon, A. C., Prouty, N. G., Roark, E.
1010 B. & van de Flierdt, T. (2014) The geochemistry of deep-sea coral skeletons: A
1011 review of vital effects and applications for palaeoceanography. Deep Sea
1012 Research Part II: Topical Studies in Oceanography. 105, p.118-118 (vol 99, pg
1013 184, 2014).
1014 Roberts, D. Long, J.B. Wilson, P.B. Mortensen, J.D. Gage, (2003) The cold-water
1015 coral *Lophelia pertusa* (Scleractinia) and enigmatic seabed mounds along the
1016 north-east Atlantic margin: are they related? Marine Pollution Bulletin 46 (2003)
1017 7-20
1018 Roberts, J.M., Wheeler, A., Freiwald, A., Cairns, S.D., 2009. Cold-Water Corals:
1019 The Biology and Geology of Deep-Sea Coral Habitats. Cambridge University
1020 Press, Cambridge.

1021 Roberts, J.M., Wheeler, A., Freiwald, A., 2006. Reefs of the deep: the biology
1022 and geology of cold-water coral ecosystems. Science 312, 543-547.
1023 Roberts, J.M., Davies, A.J., Henry, L.A., Dodds, L.A., Duineveld, G.C.A.,
1024 Lavaleye, M.S.S., Maier, C., van Soest, R.W.M., Bergman, M.J.N., Huhnerbach,
1025 V., Huvenne, V.A.I., Sinclair, D. J., Watmough, T., Long, D., Green, S.L., & van
1026 Haren., H. (2009), Mingulay reef complex: an interdisciplinary study of cold-
1027 water coral habitat, hydrography and biodiversity. Marine ecology progress
1028 series, 397, 139-151.
1029 Rüggeberg A, Dullo C, Dorschel B, Hebbeln D (2007) Environmental changes
1030 and growth history of Propeller Mound, Porcupine Seabight: evidence from
1031 benthic foraminiferal assemblages. Int J Earth Sci 96:57-72.
1032 Sánchez, F., González-Pola, C., Druet, M., García-Alegre, A., Acosta, J.,
1033 Cristobo, J., Parra, S., Ríos, P., Altuna, Á., Gómez-Ballesteros, M., Muñoz-Recio,
1034 A., Rivera, J., & del Río, G.D. (2014), Habitat characterization of deep-water
1035 coral reefs in La Gaviera Canyon (Avilés Canyon System, Cantabrian Sea). Deep
1036 Sea Research Part II: Topical Studies in Oceanography, 106, 118-140.
1037 Sarnthein, M., et al. (1995), Variations in Atlantic surface ocean
1038 paleoceanography, 50° - 80°N: A time-slice record of the last 30,000 years,
1039 Paleoceanography, 10(6), 1063-1094, doi:10.1029/95PA01453.
1040 Schmidt, F., Schmidt, A., Treguier, E., Guiheneuf, M., Moussaoui, S., Dobigeon,
1041 N., 2010. Implementation Strategies for Hyperspectral Unmixing Using Bayesian

1042 Source Separation, IEEE Transactions on Geoscience and Remote Sensing, 48,
1043 4003-4013.
1044 Schröder-Ritzau, A., Freiwald, A., & Mangini, A. (2005), U/Th-dating of deep-
1045 water corals from the eastern North Atlantic and the western Mediterranean Sea.
1046 In: Freiwald A, Roberts J.M. (eds) Cold-Water Corals and Ecosystems, Springer-
1047 Verlag, Berlin-Heidelberg, pp 1151-1169.
1048 Simpson, John J. & E. Hill, A. (1986). The Scottish Coastal Current. 295-308.
1049 10.1007/978-3-642-70886-2_21.
1050 Somoza, L., Ercilla, G., Urgorri, V., Le√≥n, R., Medialdea, T., Paredes, M.,
1051 Gonzalez, F.J., & Nombela, M.A. (2014), Detection and mapping of cold-water
1052 coral mounds and living *Lophelia* reefs in the Galicia Bank, Atlantic NW Iberia
1053 margin. Marine Geology, 349, 73-90.
1054 Thierens, M., Pirlet, H., Colin, C., Latruwe, K., Vanhaecke, F., Stuut, J.-B.,
1055 Titschack, J., Huvenne, V.A.I., Dorschel, B., Wheeler, A.J., & Henriet, J.-P.
1056 (2012), Evidence for an ice-rafting British-Irish ice sheet since the earliest
1057 Pleistocene (2.6 million years ago)): early mid-latitudinal glaciation around the
1058 North Atlantic Ocean. Quaternary Science Reviews, 44, 229-240.
1059 Thierens, M., Browning, E., Pirlet, H., Loutre, M.-F., Dorschel, B., Huvenne,
1060 V.A.I., Titschack, J., Colin, C., Wheeler, A.J. (2013). Coral-water carbonate
1061 mounds as unique palaeo-archives: the Plio-Pleistocene Challenger Mound record
1062 (NE Atlantic), Quaternary Science Reviews, 73, 14-30.
1063

1064 Thornalley, D.J., Elderfield, H., & McCave, N. (2009), Holocene oscillations in
1065 temperature and salinity of the surface subpolar North Atlantic. Nature, 457, 711-
1066 714.
1067 Thornalley, D.J.R., Blaschek, M., Davies, F.J., Praetorius, S., Oppo, D.W.,
1068 McManus, J.F., Hall, I.R., Kleiven, H., Renssen, H., McCave, I.N., (2013), Long-
1069 term variations in Iceland-Scotland overflow strength during the Holocene, Clim.
1070 Past, 9, 2073-2084.
1071 Teichert C., (1958) Cold- and Deep-Water Coral Banks AAPG Bulletin
1072 42(5):1064-1082
1073 van der Land, C., Eisele, M., Mienis, F., de Haas, H., Hebbeln, D., Reijmer, J.J.G.,
1074 & van Weering., T.C.E. (2014) Carbonate mound development in contrasting
1075 settings on the Irish margin. Deep-Sea Research Part I, Topical Studies in
1076 Oceanography, 99, 297-306.
1077 Veron JEN (1993) Corals of Australia and the Indo-Pacific. University of Hawaii
1078 Press, Honolulu, HI
1079 Victorero, L., Blamart, D., Pons-Branchu, E., Mavrogordato, M.N., Huvenne,
1080 V.A.I. (2016) Reconstruction of the formation history of the Darwin Mounds, N
1081 Rockall Trough: How the dynamics of a sandy contourite affected cold-water
1082 coral growth. Marine Geology, 378, 186-195.
1083 Waelbroeck C.; Duplessy, J-C.; Michel, E.; Labeyrie, L.; Paillard, D. Duprat, J.
1084 (2001) The timing of the last deglaciation in North Atlantic climate records,
1085 Nature volume 412, pages 724-727

1086 Waelbroeck C, et al. (2002) Sea-level and deep water temperature changes
1087 derived from benthic foraminifera isotopic records. Quat Sci Rev 21:295-305
1088 Weltje, G.J., 1997. End-member modeling of compositional data: numerical-
1089 statistical algorithms for solving the explicit mixing problem, Mathematical
1090 Geology, 29, 503-549.
1091 White, M. & Bowyer, P. The shelf-edge current north-west of Ireland Annales
1092 Geophysicae (1997) 15: 1076.
1093 White M (2007) The hydrography of the Porcupine Bank and Sea Bight and
1094 associated carbonate mounds. Int J Earth Sci 96:1-9
1095 Wienberg C., Hebbeln D., Fink H.G., Mienis F, Dorschel B., Vertino A., López-
1096 Correa M., Freiwald A. (2009). Scleractinian cold-water corals in the Gulf of
1097 Cádiz-First clues about their spatial and temporal distribution. Deep Sea Research
1098 Part I Oceanographic Research Papers. 56. 1873-1893.
1099 10.1016/j.dsr.2009.05.016.
1100 Wienberg C., Hebbeln D., Fink H.G., Mienis F, Dorschel B., Vertino A., López -
1101 Correa M., Freiwald A. (2010). Glacial cold-water coral growth in the Gulf of
1102 Cádiz: Implications of increased palaeo-productivity. Earth and Planetary Science
1103 Letters. 298. 405-416. 10.1016/j.epsl.2010.08.017.
1104 Windom, H.L. (1976) Lithogenous material in marine sediments. In: Riley J.P.,
1105 Chester R., Eds., Chemical Oceanography. Academic Press, New York, London,
1106 5:103-135.

1107 Wyville-Thomson, C., 1874. In: The Depths of the Sea. MacMillan and Co.,
1108 London, p. 527.
1109 Ziska H.; Varming, T. (2008) Palaeogene evolution of the Ymir and Wyville
1110 Thomson ridges, European North Atlantic margin Geological Society, London,
1111 Special Publications, 306, 153-168, 7 in JOHNSON, H., DORE, A. G., GATLIFF,
1112 R. W., HOLDSWORTH, R., LUNDIN, E. R. &RITCHIE, J. D. (eds) The Nature
1113 and Origin of Compression in Passive Margins. Geological Society, London,
1114 Special Publications, 306, 153-168
1115
1116
1117 Figures and Tables
1118
1119 Figure 1 : Map of the study area showing the location of vibrocore +59-07/923VE
1120 investigated in this study (yellow star). Other cores discussed in this paper are
1121 also reported in the insert (open dots) : (1) MD01-2454G; (2) Na-87-22; (3) +56-
1122 08/929VE and +56-08/930VE. Arrows represent the main subsurface
1123 oceanographic currents. NAC: North Atlantic Current; SEC: Shelf Edge Current;
1124 SCC : Scottish Coastal Current as shown in (Inall et al., 2009). The position of
1125 the maximum extent on the British Ice Sheet is show dashed line modified from
1126 Clarck et al., (2010).
1127

1128 Figure 2 : Vibrocore 59-07/293VE detailed plot of U/Th and ^{14}C dates from 0-
1129 300 cm. U/Th *L. pertusa* dates (empty circles) and ^{14}C *L. pertusa* dates (full
1130 circles) and ^{14}C benthic foraminifera *C. refulgen* dates (full squares).
1131 Sedimentation rates are estimated using ^{14}C data are (indicated on the right side
1132 of the plot (black)) and U/Th data are indicated (on the left side of the plot (bold
1133 red). Mean sedimentation rates are estimated from 160-290 cm (brown full and
1134 empty circles) and from 0-60 cm (red full and empty circles). Significant
1135 differences of sedimentation rates are observed between the U/Th and ^{14}C ages
1136 are observed in the section 160-290 cm (34.8 cm/ka for U/Th data and 70.9 cm/ka
1137 for the ^{14}C data). Similar sedimentation rates are observed in the section 0-60 cm
1138 (9.1 cm/ka for U/Th and 6.9 cm/ka for ^{14}C data).
1139
1140 Figure 3 : Vibrocore 59-07/293VE Grain-size data: A- EM1, EM2 and EM3 size
1141 distributions; B - Vibrocore 59-07/293VE grain-size data versus depth and C -
1142 Mean grain size versus depth.
1143
1144 Figure 4: Vibrocore 59-07/293VE all data versus depth. The grey band highlights
1145 the reworked zone between depth 60-160 cm with absence of well- preserved
1146 large fragments of *L pertusa* samples. From top to bottom: A: grain-size data. B:
1147 clay mineralogy. C: $\delta^{18}O$ profile of *G. bulloides* (left axis) and abundance of coral
1148 fragments > 2 cm (right axis). D: Age depth distribution in cal ka BP (U/Th (black
1149 diamonds) and ^{14}C dates for *L. pertusa* (red squares) *C. refulgens* (blue circles)

and marine bivalves (green triangles)) and right axis number of coral fragments > 2 cm. The dashed lines highlight the transitions at 300 and 400 cm discussed herein.

Figure 5 : Vibrocore 59-07/293VE all data versus age. The blue shaded area highlights the glacial age deposits > 13 cal ka BP with average mean sedimentation rate of 2 cm/ka (the age scale is compressed for easier viewing). The red shaded area highlights the end of the deglacial/early Holocene with average mean sedimentation rates of 35-8 cm/ka and the yellow shaded area highlights the period from 9 cal ka BP-modern period when abundant CWC are found and mean sedimentation is the highest: 30-40 cm/ka. From top to bottom: A: grain grain-size data. B: clay mineralogy. C: $\delta^{18}O$ and $\delta^{13}C$ profiles of *G. bulloides* of core 59-07/293VE (green and red) and Na87-22 (blue and grey). D: Age depth relationship for the stratigraphic age model (blue line) and the distribution of U/Th (black open circles) and ^{14}C dates for *L. pertusa* (full brown circles) *C. refulgens* (red squares) and marine bivalves (green triangles). The tie points for the stratigraphic age model with (blue squares). Mean sediment rates are indicated for the stratigraphic age model. The glacial section (13-50ka) of this diagram has been compressed in order to facilitate viewing of the transitions at 9 and 13 cal ka BP.

1171 Table 1 : Calibrated AMS ^{14}C age. ^{14}C ages were converted into calendar years
1172 (cal. yr BP, BP = AD 1950) by using the Marine13 calibration data set and the
1173 CALIB 7.04 program (Stuiver et al., 2005; Reimer et al., 2013). A mean reservoir
1174 effect of ~400 years has been used.
1175
1176 Table 2 : $^{230}Th/^{234}U$ ages for CWC: U and Th content, uranium isotopic initial
1177 ratio (expressed as $\delta^{234}Uo = ([^{234}U/^{238}U]_0 - 1) \times 1000$) and corrected ages for detrital
1178 fraction using ($^{230}Th/^{232}Th$) = 10 ± 4. Ages are expressed as ka before 1950.
1179
1180

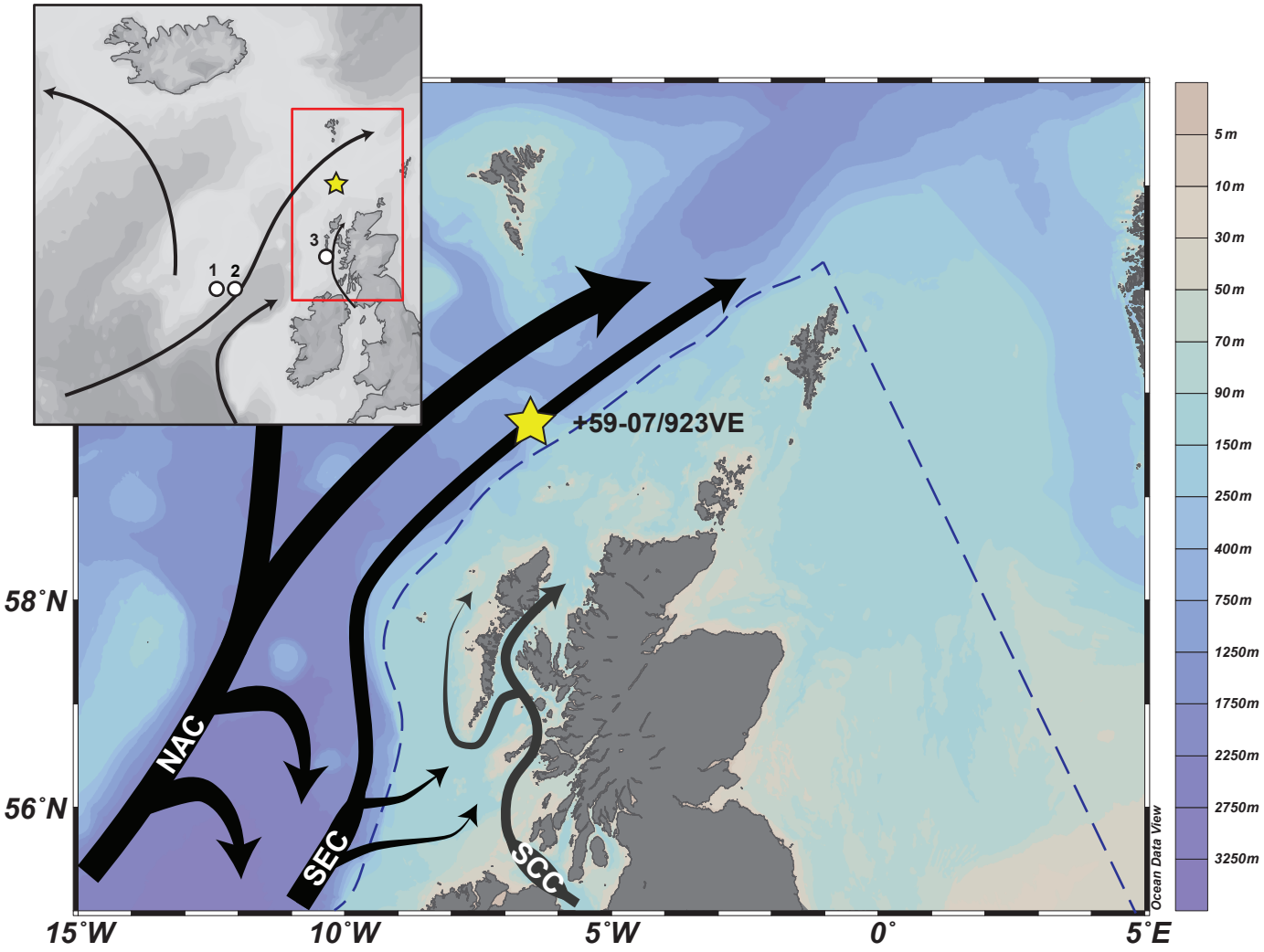
1
2
3
+59-07/923VE
NAC
SEC
SCC
58˚N
56˚N
15˚W
10˚W
5˚W
0˚
5˚E
5 m
10 m
30 m
50 m
70 m
90 m
150 m
250 m
400 m
750 m
1250 m
1750 m
2250 m
2750 m
3250 m
Ocean Data View

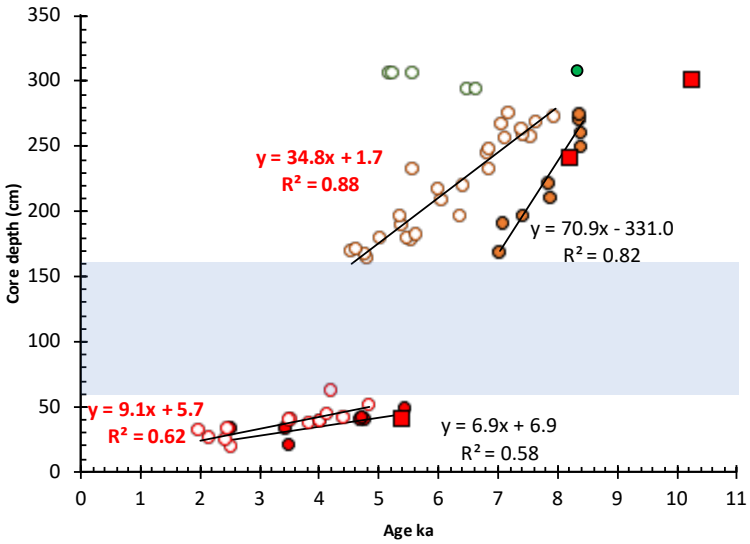
350
300
250
200
150
100
50
0
Core depth (cm)
0
1
2
3
4
5
6
7
8
9
10
11
Age ka
y = 34.8x + 1.7
R² = 0.88
y = 70.9x - 331.0
R² = 0.82
y = 9.1x + 5.7
R² = 0.62
y = 6.9x + 6.9
R² = 0.58

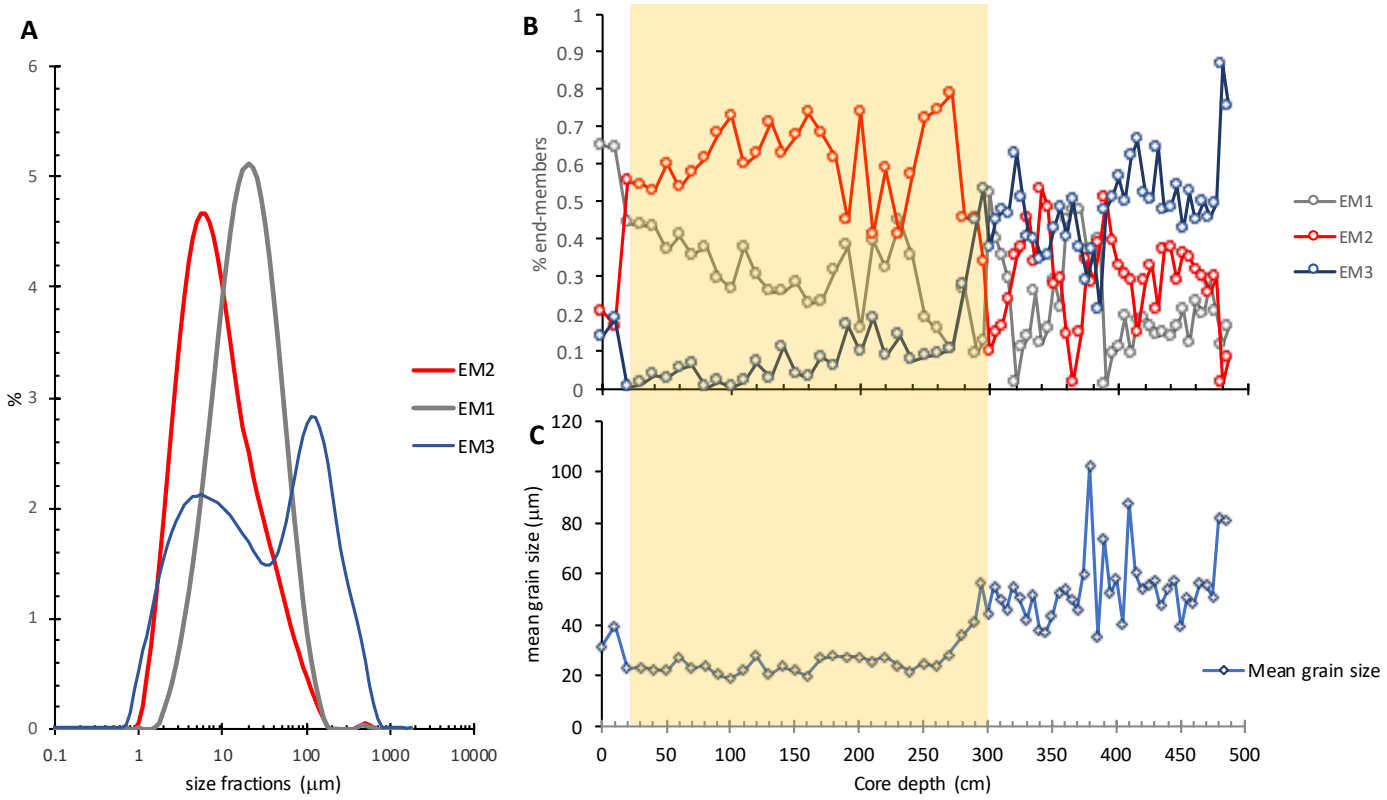
A
%
size fractions (µm)
EM2
EM1
EM3
B
% end-members
EM1
EM2
EM3
C
mean grain size (µm)
Mean grain size
Core depth (cm)

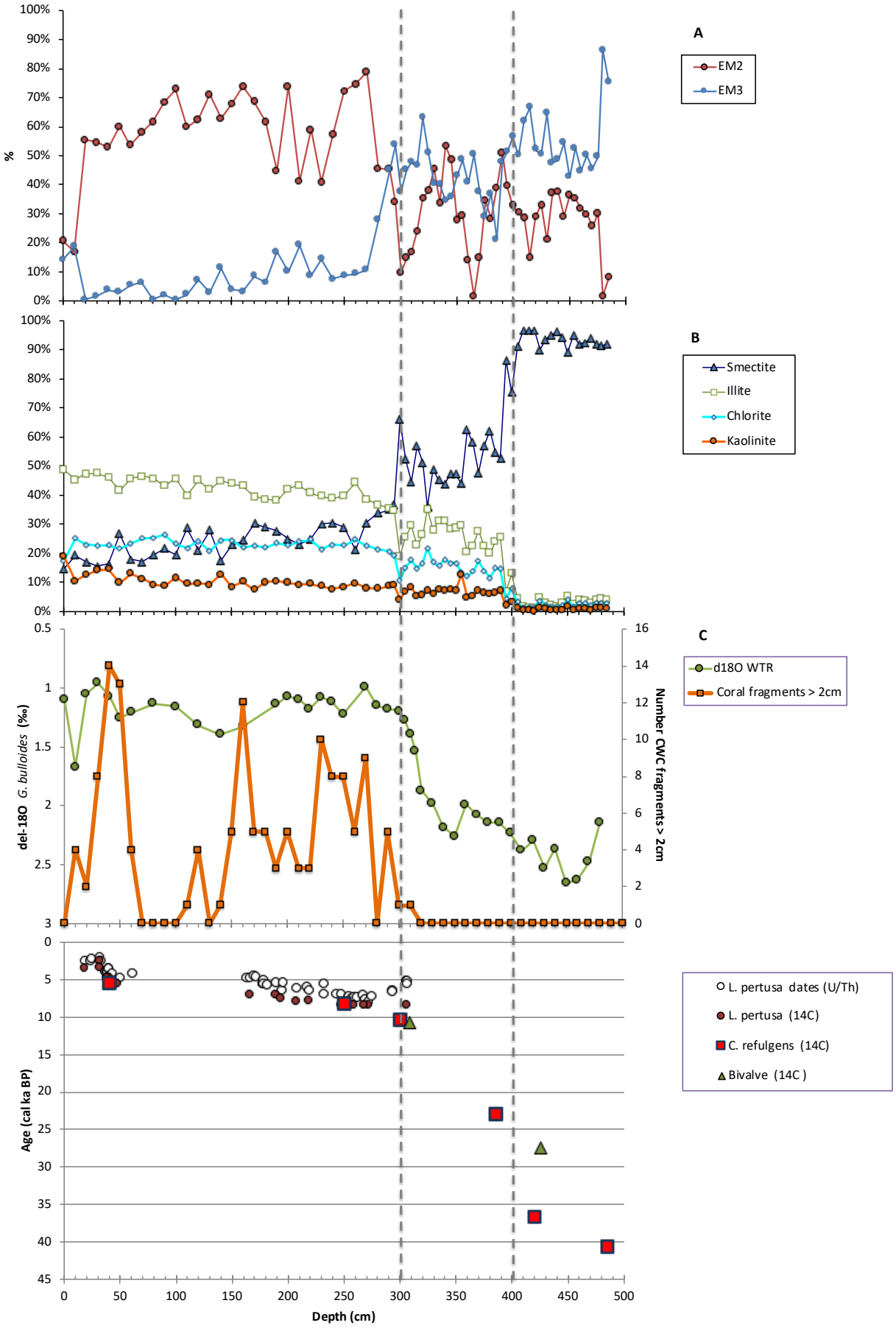
A
EM2
EM3
%
B
Smectite
Illite
Chlorite
Kaolinite
C
d18O WTR
Coral fragments > 2cm
del-18O G. bulloides (‰)
Number CWC fragments > 2cm
L. pertusa dates (U/Th)
L. pertusa (14C)
C. refulgens (14C)
Bivalve (14C)
Age (cal ka BP)
Depth (cm)

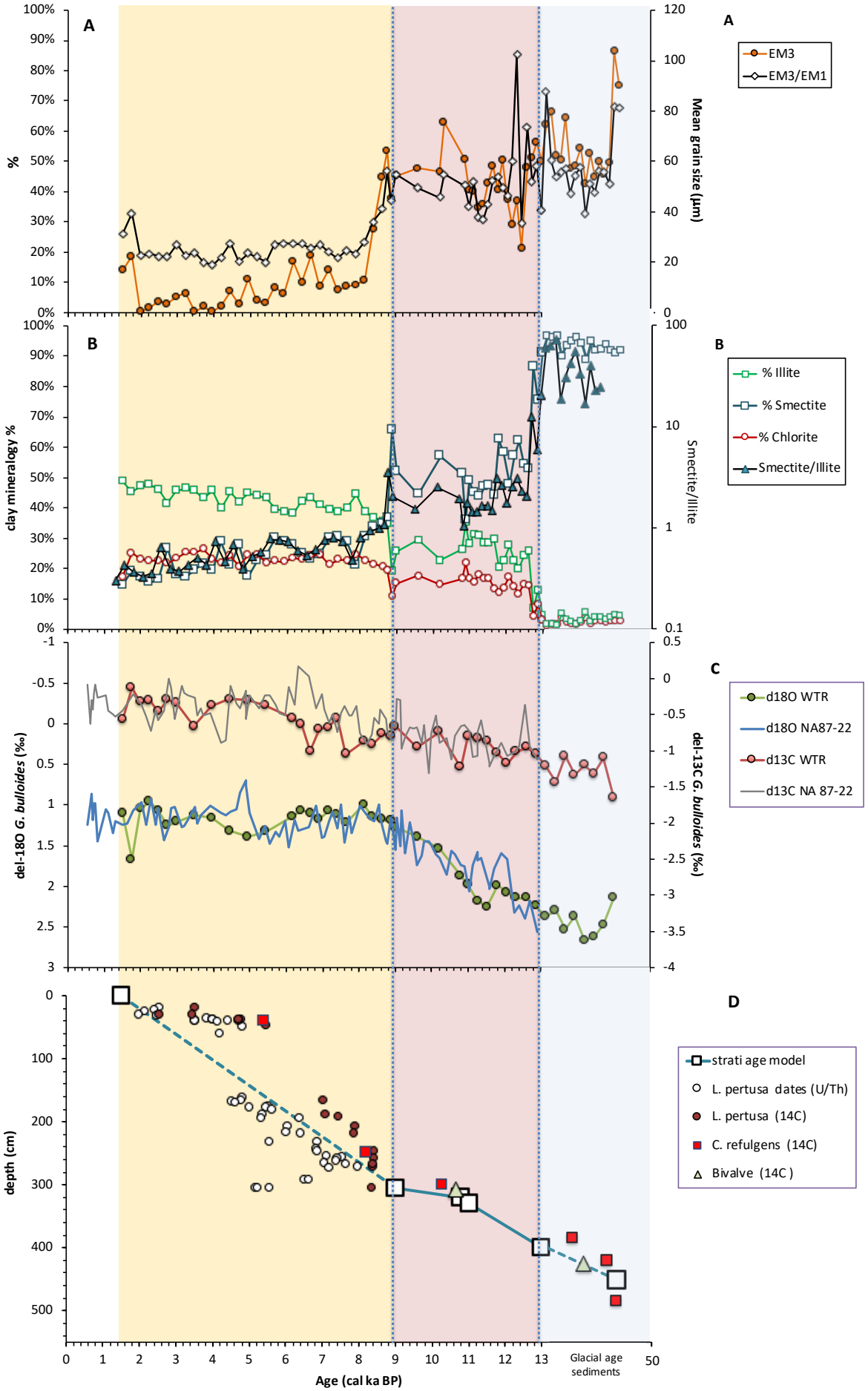
A
%
Mean grain size (µm)
EM3
EM3/EM1
B
clay mineralogy %
Smectite/Illite
% Illite
% Smectite
% Chlorite
Smectite/Illite
C
del-18O G. bulloides (‰)
del-13C G. bulloides (‰)
d18O WTR
d18O NA87-22
d13C WTR
d13C NA 87-22
D
depth (cm)
strati age model
L. pertusa dates (U/Th)
L. pertusa (14C)
C. refulgens (14C)
Bivalve (14C)
Age (cal ka BP)
Glacial age sediments

N° GifA / SacA	Depth (cm)	species	Age BP	Err âge BP (1σ)	Cal years BP Median Probability	2 σ range cal years BP	
14366 / 40200	19	*L pertusa*	3625	35	**3522**	cal BP 3424 - 3627	
14367 / 40201	31.5	*L pertusa*	2800	30	**2557**	cal BP 2423 - 2682	
15305 / 42891	32	*L pertusa*	3575	30	**3465**	cal BP 3378 - 3554	*
14368 /40202	38.5	*L pertusa*	4580	30	**4805**	cal BP 4689 - 4863	
15306 / 42892	39	*L pertusa*	4520	30	**4730**	cal BP 4612 - 4817	*
14369 / 40203	41	*L pertusa*	4525	30	**4736**	cal BP 4618 - 4820	
15308 / 42894	48	*L pertusa*	5100	30	**5470**	cal BP 5332 - 5338	*
14371 / 40205	166.5	*L pertusa*	6530	40	**7047**	cal BP 6929 - 7155	
14372 / 40206	189	*L pertusa*	6590	35	**7115**	cal BP 6999 - 7217	
15309 / 42895	194	*L pertusa*	6945	30	**7450**	cal BP 7394 - 7524	*
14373 / 40207	208	*L pertusa*	7450	40	**7911**	cal BP 7819 - 7995	
14374 / 40208	219	*L pertusa*	7415	40	**7880**	cal BP 7819 - 7995	
14376 / 40210	247	*L pertusa*	7985	50	**8443**	cal BP 8346 - 8552	
14377 / 40211	258.5	*L pertusa*	7990	45	**8447**	cal BP 8357 - 8548	
15310 /42896	268	*L pertusa*	7945	30	**8400**	cal BP 8335 - 8485	*
14378 / 40212	272	*L pertusa*	7960	40	**8417**	cal BP 8357 - 8548	
14379 / 40213	306	*L pertusa*	7920	45	**8381**	cal BP 8357 - 8548	
15312 / 42898	40	*C. refulgens*	5060	30	**5410**	cal BP 4612 - 4817	*
15313 / 42899	250	*C. refulgens*	7745	30	**8220**	cal BP 8144 - 8309	*
15314 / 42900	300	*C. refulgens*	9440	30	**10271**	cal BP 10196 - 10383	*
15315 / 42901	385	*C. refulgens*	19430	70	**22905**	cal BP 22619 - 23160	*
15317 / 42903	420	*C. refulgens*	33080	270	**36643**	cal BP 35998 - 37633	*
15318 / 42904	485	*C. refulgens*	36430	390	**40655**	cal BP 39804 - 41461	*
15319 / 42905	308	*V. casima*	9750	35	10650	cal BP 10196 - 10383	*
15320 / 42906	425	*Venus sp.*	23490	100	**27396**	cal BP 27171 - 27603	*
15321 / 42907	480	*Venus sp.*	48800	1700	**>50000**		

Lab-code	sample-label	mean depth (cm)	[^{238}U] (ppm)		[^{232}Th] (ppm)		$\delta^{234}U_m$ (‰)		$^{230}Th/^{238}U$		$^{230}Th/^{232}Th$		$\delta^{234}U(0)$ (‰)		age (kyr)		age (kyr) Cor BP	
5426	18-20	19	4.238	0.004	0.1407	0.0004	145.6	0.7	0.0273	0.0001	2639.4	13.3	146.6	0.7	2.63	0.02	2.555	0.019
5428	23-25	24	3.775	0.004	0.2042	0.0005	145.9	0.7	0.0261	0.0002	1551.6	9.9	146.9	0.7	2.52	0.02	2.437	0.024
5427	21-29	25	3.552	0.004	0.1099	0.0003	145.9	0.7	0.0233	0.0001	2414.1	14.4	146.8	0.8	2.24	0.01	2.166	0.019
5268	*29-34*	*31.5*	4.189	0.007	0.1067	0.0003	*145.9*	*1.0*	0.0216	0.0001	*2639.6*	*13.2*	*146.8*	*1.0*	*2.08*	*0.01*	*2.004*	*0.015*
5429	32-33	32.5	4.432	0.007	0.2132	0.0004	146.1	0.8	0.0266	0.0003	1777.7	18.8	147.2	0.8	2.56	0.03	2.482	0.035
5592	36-38	37	3.899	0.007	0.1459	0.0006	145.2	1.2	0.0404	0.0002	3408.1	18.6	146.9	1.2	3.92	0.03	3.846	0.030
5703	37-39	38	3.949	0.012	0.1597	0.0008	145.6	1.3	0.0423	0.0003	3319.4	22.1	147.3	1.3	4.11	0.03	4.033	0.037
5267	*37-40*	*38.5*	3.517	0.007	0.1353	0.0006	*145.4*	*0.8*	0.0422	0.0002	*3427.3*	*15.3*	*147.1*	*0.8*	*4.10*	*0.02*	*4.021*	*0.026*
5704bis	*39-41*	*40*	4.147	0.015	0.1684	0.0008	*143.3*	*1.0*	0.0372	0.0002	*2896.5*	*17.1*	*144.8*	*1.1*	*3.61*	*0.02*	*3.533*	*0.030*
5704	*39-41*	*40*	4.125	0.006	0.1746	0.0010	*148.5*	*0.6*	0.0373	0.0002	*2832.5*	*15.4*	*150.0*	*0.6*	*3.60*	*0.02*	*3.523*	*0.027*
5266	*40-42*	*41*	3.552	0.004	0.1199	0.0003	*146.4*	*0.8*	0.0465	0.0002	*4400.0*	*19.0*	*148.3*	*0.8*	*4.52*	*0.02*	*4.445*	*0.027*
5593	40-46	43	3.783	0.005	0.3153	0.0012	144.9	0.6	0.0437	0.0002	1657.9	8.7	146.6	0.6	4.25	0.02	4.158	0.035
5265	*48-52*	*50*	3.181	0.007	0.1936	0.0008	*145.5*	*0.6*	0.0505	0.0002	*2608.9*	*8.8*	*147.6*	*0.6*	*4.92*	*0.02*	*4.841*	*0.027*
5594	60-63	61.5	3.406	0.007	0.1809	0.0008	144.8	0.8	0.0441	0.0002	2627.6	14.4	146.6	0.8	4.29	0.03	4.207	0.034
5264	*161-166*	*163.5*	4.123	0.004	0.2157	0.0007	*145.4*	*0.7*	0.0503	0.0002	*3014.5*	*11.6*	*147.4*	*0.7*	*4.90*	*0.02*	*4.820*	*0.028*
5263	*165-168*	*166.5*	3.838	0.006	0.3510	0.0011	*145.1*	*0.6*	0.0502	0.0002	*1712.7*	*6.7*	*147.1*	*0.6*	*4.89*	*0.02*	*4.801*	*0.033*
5705	*168-170*	*169*	3.907	0.006	0.2673	0.0008	*144.2*	*0.7*	0.0475	0.0002	*2230.8*	*8.0*	*146.1*	*0.7*	*4.63*	*0.02*	*4.542*	*0.028*
5595	170-172	171	4.191	0.008	0.3109	0.0028	144.3	0.9	0.0486	0.0005	2054.7	23.1	146.3	0.9	4.74	0.06	4.649	0.067
5262	*175-179*	*177*	3.465	0.004	0.2475	0.0009	*145.9*	*0.6*	0.0576	0.0003	*2530.2*	*11.3*	*148.2*	*0.6*	*5.63*	*0.03*	*5.542*	*0.038*
5707	*178-179*	*178.5*	3.502	0.005	0.3701	0.0011	*145.3*	*0.6*	0.0526	0.0002	*1605.6*	*5.3*	*147.4*	*0.6*	*5.13*	*0.02*	*5.039*	*0.033*
5706	*175-182*	*178.5*	3.544	0.004	0.1933	0.0002	*146.1*	*0.9*	0.0571	0.0001	*3198.8*	*6.3*	*148.4*	*0.9*	*5.58*	*0.02*	*5.497*	*0.023*
5596	180-182	181	3.349	0.008	0.3901	0.0017	143.8	0.9	0.0587	0.0003	1582.8	7.4	146.2	0.9	5.75	0.03	5.645	0.046
5261	*187-191*	*189*	3.669	0.007	0.9898	0.0038	*143.1*	*0.7*	0.0566	0.0003	*658.1*	*3.7*	*145.3*	*0.7*	*5.54*	*0.04*	*5.396*	*0.068*
5708	*194-196*	*195*	4.019	0.009	0.2034	0.0029	*145.3*	*1.1*	0.0658	0.0009	*4135.4*	*59.9*	*147.9*	*1.1*	*6.45*	*0.10*	*6.375*	*0.108*
5260	*194-198*	*196*	4.120	0.008	0.1098	0.0005	*143.9*	*0.8*	0.0556	0.0003	*6527.3*	*31.3*	*146.2*	*0.8*	*5.44*	*0.03*	*5.364*	*0.034*
5259	*206-210*	*208*	4.127	0.008	0.2235	0.0008	*144.0*	*0.8*	0.0628	0.0002	*3631.1*	*13.3*	*146.5*	*0.8*	*6.16*	*0.03*	*6.075*	*0.034*
5709	*215-219*	*217*	4.216	0.008	0.2455	0.0009	*145.6*	*0.8*	0.0623	0.0003	*3405.6*	*14.9*	*148.1*	*0.8*	*6.10*	*0.03*	*6.024*	*0.039*
5258	*217-221*	*219*	4.264	0.010	0.3412	0.0015	*145.1*	*0.8*	0.0664	0.0003	*2596.8*	*13.1*	*147.8*	*0.8*	*6.52*	*0.04*	*6.427*	*0.048*
5257	*231-233*	*232*	4.509	0.018	0.3317	0.0013	*144.5*	*1.0*	0.0579	0.0002	*2462.5*	*8.6*	*146.8*	*1.0*	*5.66*	*0.03*	*5.578*	*0.035*
5710	*230-234*	*232*	3.563	0.008	0.1546	0.0024	*142.0*	*0.8*	0.0705	0.0004	*5160.8*	*28.3*	*144.9*	*0.9*	*6.95*	*0.04*	*6.876*	*0.050*

5597	241-246	243.5	3.620	0.018	0.1612	0.0009	142.6	1.3	0.0701	0.0005	4929.1	34.0	145.4	1.4	6.91	0.06	6.829	0.063
5256	*245-249*	*247*	3.684	0.005	0.2832	0.0014	*146.1*	*0.7*	0.0708	0.0003	*2881.8*	*12.2*	*149.0*	*0.7*	*6.96*	*0.03*	*6.872*	*0.045*
5711	*253-257*	*255*	3.727	0.006	0.5141	0.0016	*146.9*	*1.1*	0.0737	0.0003	*1715.4*	*7.4*	*149.9*	*1.1*	*7.24*	*0.04*	*7.134*	*0.055*
5712	*255-258*	*256.5*	3.857	0.011	0.3328	0.0013	*143.6*	*1.2*	0.0775	0.0003	*2846.4*	*12.7*	*146.8*	*1.2*	*7.65*	*0.04*	*7.562*	*0.054*
5255	*257-260*	*258.5*	3.310	0.005	0.1561	0.0006	*144.3*	*0.7*	0.0761	0.0003	*5050.5*	*20.8*	*147.4*	*0.7*	*7.51*	*0.04*	*7.429*	*0.043*
5713	*260-264*	*262*	3.298	0.009	0.2888	0.0020	*145.6*	*1.4*	0.0761	0.0006	*2755.8*	*21.0*	*148.7*	*1.4*	*7.50*	*0.07*	*7.405*	*0.079*
5714	265-268	266.5	3.404	0.009	0.3629	0.0013	142.8	1.2	0.0726	0.0004	2162.2	11.7	145.7	1.2	7.16	0.05	7.066	0.061
5598	267-270	268.5	3.942	0.013	0.4034	0.0017	142.9	1.2	0.0785	0.0003	2413.1	10.7	146.1	1.2	7.76	0.04	7.660	0.056
5254	*269-275*	*272*	3.490	0.005	0.2753	0.0010	*144.5*	*0.6*	0.0815	0.0003	*3234.3*	*12.5*	*147.8*	*0.6*	*8.05*	*0.04*	*7.966*	*0.046*
5253	*272-278*	*275*	4.021	0.028	0.3347	0.0029	*144.7*	*0.7*	0.0741	0.0002	*2739.3*	*6.9*	*147.7*	*0.7*	*7.30*	*0.02*	*7.209*	*0.034*
5252	*291-295*	*293*	3.670	0.008	0.3228	0.0005	*144.5*	*1.1*	0.0672	0.0002	*2354.6*	*8.3*	*147.2*	*1.1*	*6.60*	*0.02*	*6.514*	*0.034*
5430	291-295	293	3.820	0.006	0.1289	0.0003	144.2	0.9	0.0685	0.0003	6536.4	25.0	146.9	0.9	6.74	0.03	6.662	0.036
5431	305-306	305.5	4.482	0.006	0.2389	0.0007	144.6	0.8	0.0541	0.0003	3248.9	15.5	146.8	0.8	5.28	0.03	5.204	0.036
5432	305-307 b	306	4.166	0.006	0.1602	0.0007	144.6	1.0	0.0545	0.0003	4539.4	22.1	146.8	1.0	5.33	0.03	5.250	0.036
5251	*305-307*	*306*	4.052	0.008	0.3649	0.0005	*145.2*	*1.0*	0.0582	0.0001	*1989.6*	*4.5*	*147.5*	*1.0*	*5.69*	*0.02*	*5.594*	*0.029*